Cell Reports

Article

Typhoid toxin hijacks Wnt5a to establish host senescence and *Salmonella* infection

Graphical abstract

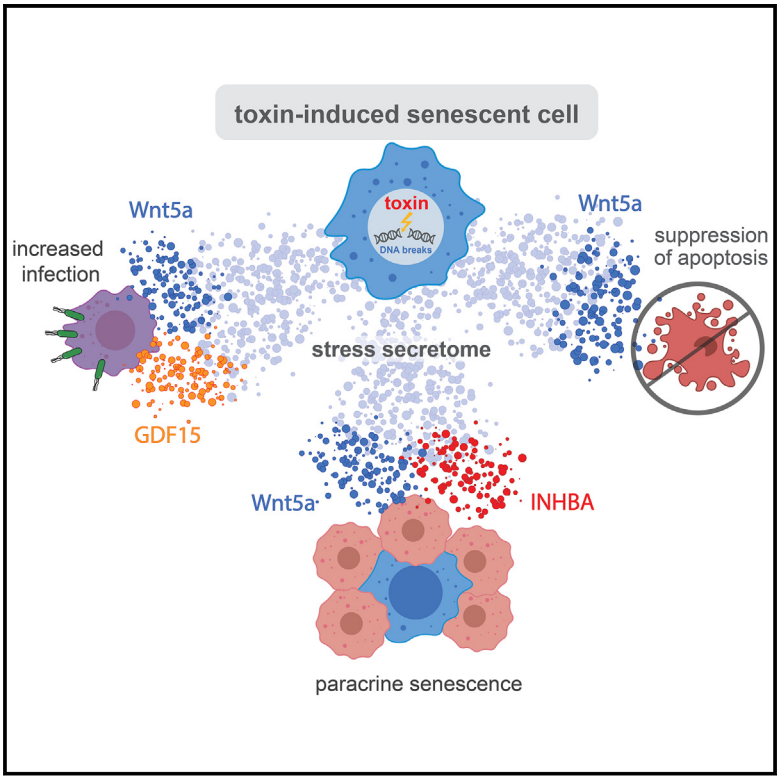

Highlights

- *Salmonella* co-opts Wnt5a, INHBA, and GDF15 secreted from toxin-induced senescent cells
- Wnt5a suppresses apoptosis, establishing senescence in response to typhoid toxin
- Wnt5a and INHBA synergize, causing paracrine senescence in bystander cells
- *Salmonella* hijacks secreted factors Wnt5a and GDF15 to enhance host cell invasion

Authors

Mohamed ElGhazaly, Mark O. Collins, Angela E.M. Ibler, Daniel Humphreys

Correspondence

d.humphreys@sheffield.ac.uk

In brief

ElGhazaly et al. reveal how *Salmonella enterica* hijacks a tumor-suppressor mechanism. By uncovering the secreted proteome of human cells undergoing acute senescence in response to typhoid toxin of *Salmonella*, they show that Wnt5a suppresses apoptosis, enabling senescence while synergizing with INHBA and GDF15 to mediate paracrine senescence and infections.

ElGhazaly et al., 2023, Cell Reports *42*, 113181
October 31, 2023
https://doi.org/10.1016/j.celrep.2023.113181

CellPress

Cell Reports

CellPress
OPEN ACCESS

Article

Typhoid toxin hijacks Wnt5a to establish host senescence and *Salmonella* infection

Mohamed ElGhazaly,[1] Mark O. Collins,[1] Angela E.M. Ibler,[1] and Daniel Humphreys[1,2,*]
[1]School of Biosciences, University of Sheffield, Sheffield, South Yorkshire S10 2TN, UK
[2]Lead contact
*Correspondence: d.humphreys@sheffield.ac.uk
https://doi.org/10.1016/j.celrep.2023.113181

SUMMARY

Damage to our genome causes acute senescence in mammalian cells, which undergo growth arrest and release a senescence-associated secretory phenotype (SASP) that propagates the stress response to bystander cells. Thus, acute senescence is a powerful tumor suppressor. *Salmonella enterica* hijacks senescence through its typhoid toxin, which usurps unidentified factors in the stress secretome of senescent cells to mediate intracellular infections. Here, transcriptomics of toxin-induced senescent cells (TxSCs) and proteomics of their secretome identify the factors as Wnt5a, INHBA, and GDF15. Wnt5a establishes a positive feedback loop, driving INHBA and GDF15 expression. In fibroblasts, Wnt5a and INHBA mediate autocrine senescence in TxSCs and paracrine senescence in naive cells. Wnt5a synergizes with GDF15 to increase *Salmonella* invasion. Intestinal TxSCs undergo apoptosis without Wnt5a, which is required for establishing intestinal TxSCs. The study reveals how an innate defense against cancer is co-opted by a bacterial pathogen to cause widespread damage and mediate infections.

INTRODUCTION

Damage to our genome can generate double-strand DNA breaks (DSBs), resulting in gene mutations with oncogenic potential. To counteract pathology, the DNA damage response (DDR) is activated through the kinases ATM (ataxia telangiectasia mutated), which responds to DSBs, and ATR (ATM and rad3-related), which senses single-strand DNA breaks (SSBs).[1] Uniting the functions of ATM and ATR is phosphorylation of histone H2AX at S139 (γH2AX),[2,3] which recruits DDR proteins at sites of damage to coordinate repair and cell-fate decisions including survival, apoptosis, and senescence.[1,4–6]

Cellular senescence is a hallmark of aging that restricts the growth of cells with genomic stress through stable cell-cycle arrest.[7,8] Senescent cells display persistent γH2AX and 53BP1 DDRs, elevated expression of cyclin-dependent kinase (CDK) inhibitors (e.g., p16, p21), loss of hyperphosphorylated retinoblastoma protein (*p*-pRb), and increased lysosomal content marked by senescence-associated β-galactosidase (SA-β-Gal).[7,8] Senescent cells release a signature pro-inflammatory secretome that establishes a senescence-associated secretory phenotype (SASP).[8–10] SASP factors modulate the microenvironment to enforce autocrine senescence in senescent cells while establishing paracrine senescence in naive bystander cells.[9,11,12] The factors also recruit immune cells to eliminate damaged cells with pathological potential.[13–15] Consequently, acute senescence is a powerful tumor suppressor.[7,8] However, persistent DDRs cause chronic SASPs, and the resulting inflammation promotes age-related pathologies such as cancer. For example, DNA damage caused by the toxin colibactin of *Escherichia coli* induced a SASP that promoted colon tumor growth.[16] While the DDR is best known for preventing proliferation of cancerous cells,[6] the DDR continues to be revealed as an important innate defense against intracellular bacterial infections.[17,18] Thus, bacterial pathogens have evolved sophisticated ways to manipulate host DDRs and execute their virulence strategies.[7,19] This is exemplified by genotoxic serovars of *Salmonella enterica*, particularly the human pathogen *S.* Typhi, which causes 14 million cases of acute typhoid fever per year and asymptomatic, often lifelong, chronic infections in individuals who suffer increased risk of gallbladder carcinoma.[20]

To cause typhoid and chronic disease, *S.* Typhi establishes intracellular intestinal infections and evades innate immune responses before disseminating to systemic sites.[20] Intracellular *S.* Typhi resides within the *Salmonella*-containing vacuole from where it expresses the typhoid toxin comprising PltB-PltA-CdtB subunits that is exocytosed into the extracellular milieu.[21] Once deployed, the PltB subunit binds to sialylated glycans on host surface receptors, facilitating toxin endocytosis.[22] Reduction of disulfide bonds linking PltA-CdtB liberates the toxigenic DNase1-like subunit CdtB, which translocates to the nucleus, where it activates DDRs through nuclease activity.[21–24] The toxin is also encoded by related *Salmonella* serovars including *S.* Paratyphi and *S.* Javiana, which cause disease in humans and food-chain animals worldwide.[25,26] Toxin-induced DDRs are implicated in *Salmonella* evasion of intestinal inflammatory responses,[26,27] typhoid fever,[22,28] bacteraemia,[28] dissemination,[26,27] and chronic infection.[27] The mechanisms by which toxin-induced DDRs mediate *Salmonella* infections are unclear.

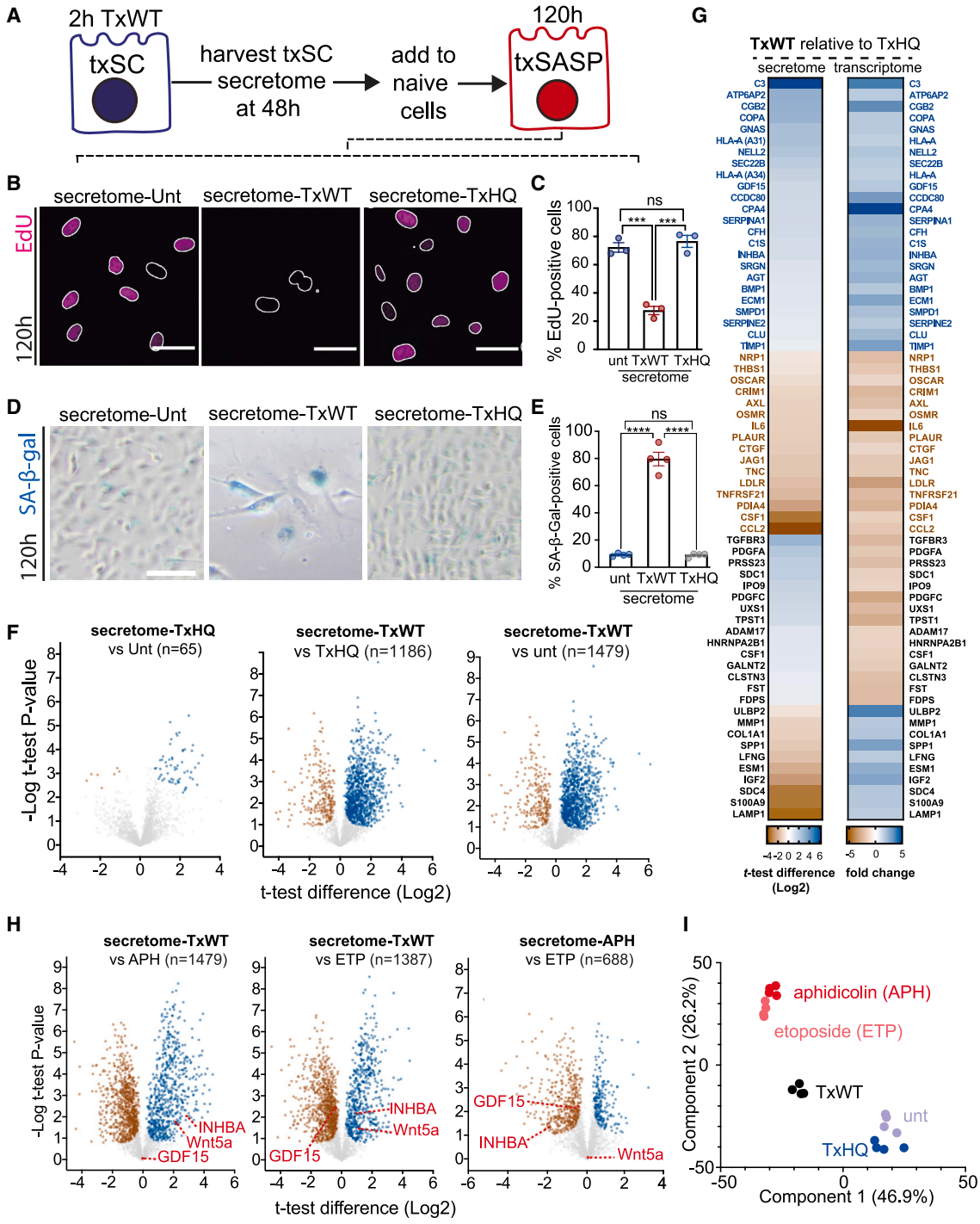

Figure 1. The typhoid-toxin-induced host secretome underlying txSASP

(A) Experimental schematic.

(B) HT1080 cells undergoing replication of EdU-labeled DNA (magenta) 120 h after incubation with secretome-Unts, secretome-TxWT, or secretome-TxHQs harvested between 0 and 48 h in complete growth medium. Outlines of DAPI-stained nuclei indicated. Scale bar represents 50 μm.

(C) Quantification of (B) using quantification protocol 1 (Q1), n = 3.

(D and E) Paracrine SA-β-Gal in cells from experiment described in (B) using pooled secretomes harvested in serum-free conditions (D), and its quantification (E). Scale bar represents 100 μm. Q6 (n = 4).

(F) Volcano plots indicating significantly up-regulated (blue dots) and down-regulated (brown) proteins in secretomes harvested as described in (C). Perseus two-sample t test (s0 = 0.01 and false discovery rate [FDR] = 0.05). n = 4.

(legend continued on next page)

Typhoid toxin was shown to induce acute cellular senescence in cultured fibroblasts[23] and in the intestinal mucosa and T lymphocytes of infected mice.[24,29] Senescence was caused by two distinct DDRs: DSBs marked by ATM-dependent canonical γH2AX foci and SSBs signified by ATR-dependent pan-γH2AX localization throughout the nucleus.[23] *Salmonella* hijacked senescence to promote intracellular infections. This was dependent upon an unidentified toxin-induced secretome released from senescent cells, which transmitted senescence to bystander cells indicative of toxin-induced SASPs (txSASPs). Unlike many viruses, pathogenic bacteria do not depend on host cell proliferation to replicate, so how senescence might counteract infection is unclear. Instead, senescence may enable subversion of the host secretome that can remodel bystander cells in the infection niche.[7]

The human host secretome plays a critical part in determining the outcome of bacterial infections.[30–33] However, host secretome responses to a bacterial toxin have not yet been resolved. Here, we sought to determine the identity of the toxin-induced host secretome from senescent cells underlying txSASPs to further address the significance of senescence in bacterial infections. The study identifies Wnt5a and transforming growth factor β (TGF-β) ligands INHBA and GDF15 in the toxin-induced host secretome of senescent cells. Wnt5a synergized with INHBA and GDF15 to enforce senescence and host cell infections. Wnt5a displayed a cell-type-dependent role in intestinal cells, where it enabled senescent cells to evade apoptosis. The study reveals how a bacterial toxin induces a stress secretome through DDRs to rewire the host and enhance infections.

RESULTS

The host cell secretome in response to acute senescence from typhoid toxin

Unidentified factors in the secretome of intoxicated cells were shown to underlie txSASPs, which enhanced infection and caused paracrine senescence in bystander cells.[23] Thus, we reasoned that investigating toxin-induced senescent cells (TxSCs) and their secretome at 48 h would form a basis to understand the effects of txSASPs by assaying paracrine senescence in naive bystander cells at 120 h. To identify the factors underlying txSASPs, we first generated TxSCs using established protocols[23] as depicted in Figures 1A and S1A: HT1080 fibroblasts were intoxicated for 2 h with 20 ng/mL WT purified recombinant typhoid toxin (TxWT), which resulted in stalled synthesis of EdU-labeled DNA due to cell-cycle arrest by 48 h (Figures S1B and S1C). Senescence responses continued to establish at 96 h, marked by growth arrest and up-regulation of SA-β-Gal (Figures S1D and S1E). This contrasted with untreated control cells (Unts) or cells treated with toxin lacking DNase activity due to a H160Q mutation in CdtB (TxHQs) that progressed through the cell cycle and lacked SA-β-Gal (Figures S1C–S1E). We found that TxSCs continued to adopt signatures of senescence including persistent γH2AX responses and nuclear distension (Figures S1F–S1H). To further test TxSC responses at 48 h, we sought to determine whether prolonged incubation with the secretome from TxSCs (secretome-TxWT) induces paracrine senescence as previously reported.[23] Secretome-TxWT harvested at 48 h was incubated with naive bystander HT1080 fibroblasts for 120 h (Figure 1A). Secretome-TxWT, but not control secretomes from untreated cells (secretome-Unts) or TxHQ-treated cells (secretome-TxHQs), caused paracrine senescence as determined by cell-cycle arrest (Figures 1B and 1C).

To characterize the proteome of secretome-TxWT, we cultured TxWT-treated cells in the absence of serum to avoid plasma proteins in downstream proteomic analysis (workflow in Figure S2A). We confirmed DDR activation in serum-free TxWT-treated cells and paracrine senescence by secretome-TxWT harvested in batches between 0 and 48 h (Figures S2B–S2G). The pooled secretome-TxWT induced cellular distension and increased SA-β-Gal activity in naive bystander cells, confirming paracrine senescence (Figures 1D and 1E). Quantitative liquid chromatography-tandem mass spectrometry (LC-MS/MS) analysis enabled unbiased identification of proteins in secretome-Unts, secretome-TxHQs, and secretome-TxWT (Figure 1F). There were few protein abundance differences between negative control secretome-Unts and secretome-TxHQs (n = 65 significant proteins), which contrasted with secretome-TxWT that was significantly divergent from secretome-Unts (n = 1,479) and secretome-TxHQs (n = 1,186). The majority of significant proteins were up-regulated in secretome-TxWT (Figure 1F; 954 proteins out of 1,186 indicated with blue circles in TxWT vs. TxHQs), which was also observed in the secretome of cells undergoing irradiation- and oncogene-induced senescence.[34] All typhoid toxin subunits were identified in our input material of recombinant TxWT (Figure S2H), which was consistent with the reported 1 CdtB:1 PltA:5 PltB stoichiometry.[22] However, no peptides for typhoid toxin subunits CdtB or PltA were identified in the proteomic analysis of secretomes (Figure S2H), though we observed the non-toxigenic subunit PltB, presumably bound to recycled receptors shed from the cell surface. Thus, the paracrine effects on bystander cells originate from secreted host proteins identified in secretome-TxWT rather than any remaining typhoid toxin. Figure S2I reveals secretome-TxWT from senescent cells comprising 133 proteins, which were defined by their presence within the human secretome[35,36] and

(G) Heatmap analyzing expression of factors in TxWT-induced secretome relative to TxHQ-treated cells at 48 h determined by GeneChip microarray transcriptome analysis ($p < 0.05$). Blue text indicates up-regulated and brown down-regulated, and black text indicates opposing fold changes between analyses.
(H) Volcano plots indicating significantly increased (blue dots) and decreased (brown) protein abundance in secretomes harvested from TxWT-, aphidicolin-, or etoposide-treated cells harvested between 0 and 48 h post-treatment. Perseus two-sample t test (s0 = 0.01 and FDR = 0.05) from 4 biological repeats. Red labels indicate Wnt5a, INHBA, and GDF15.
(I) Principal-component analysis of secretomes described in (H).
In (C) and (E), asterisks indicate significance calculated by one-way ANOVA with Tukey's multiple comparison test. Data represented as mean ± standard error of the mean (SEM). *$p < 0.05$, **$p < 0.01$, ***$p < 0.001$, ****$p < 0.0001$, ns denotes non-significance.
See also Figures S1–S3.

their differential regulation relative to negative controls ($p < 0.05$, n = 133 significant proteins).

Toxin-induced host secretome implicates TGF-β signaling in cellular senescence

To further define secretome-TxWT, the transcriptome of TxSCs was determined by GeneChip microarray transcriptome analysis of cells at 48 h following 2 h treatment with TxWT or TxHQs (Figure 1G). Of the 133 proteins comprising secretome-TxWT (Figure S2I), 64 proteins were identified as significant by both proteomics and transcriptomics (Figure 1G). Secretome-TxWT included known SASP proteins such as effectors of innate immunity (e.g., complement C3, C1r, and C1s) that were up-regulated in both analyses (blue labeling), as were SERPIN-A1, ECM1, and TIMP1, which were identified in the SASP Atlas database.[34] Of the proteins that were down-regulated in both proteomic and transcriptomic analyses (brown labeling), the most notable was interleukin-6 (IL-6), which is implicated in SASP.[7,8,10] TGF-β ligands INHBA (also known as activin A), GDF15, and BMP1 were found up-regulated in both analyses (Figure 1G). Interestingly, inhibitors of INHBA-driven TGF-β signaling, TGFBR3 and follistatin (FST), were found up-regulated by proteomics but down-regulated by transcriptomics (black labeling), perhaps suggesting that the receptor TGFBR3, for example, is shed from TxSCs rather than exhibiting increased expression. Indeed, the sheddase ADAM17 was also up-regulated, which is implicated in liberating cell-surface-bound SASP proteins during oncogene-induced senescence.[8]

We next determined whether txSASP is transmitted through up-regulated or down-regulated proteins in secretome-TxWT. When we replenished the down-regulated proteins in secretome-TxWT by supplementing with secretome-Unts or secretome-TxHQs, elevated SA-β-Gal was still observed at 120 h, indicating that paracrine senescence is mediated via up-regulated proteins in secretome-TxWT (Figures S3A and S3B). This reinforced our interest in TGF-β-family ligands up-regulated in secretome-TxWT (e.g., INHBA, GDF15, and BMP1 in Figure 1G). Indeed, PANTHER gene-function analysis identified 3 proteins that converge on TGF-β signaling in secretome-TxWT relative to secretome-TxHQs (Figure S3C).

Typhoid toxin induces expression of txSASP factors Wnt5a, INHBA, and GDF15

The TGF-β signaling pathway represents a major axis in oncogene-induced transmissible senescence.[8,12,14,37] Thus, our data indicate a conserved role for TGF-β ligands in senescence triggered by divergent DNA damage inducers that include typhoid toxin. To investigate this further, we treated cells with TxWT, the SSB-inducer aphidicolin (APH), or the DSB-inducer etoposide (ETP)1 before examining senescence responses. Like TxWT, we found that APH and ETP both induced senescence-like responses marked by γH2AX and SA-β-Gal (Figure S3D) and paracrine senescence in ∼40% of naive cells demonstrating SASP (Figure S3E). Quantitative LC-MS/MS analysis showed secretome-TxWT was significantly divergent from secretome-APH (1,479 proteins) and secretome-ETP (1,387 proteins), while secretome-APH and secretome-ETP had more overlap, with only 688 differentially regulated proteins (Figure 1H). Indeed, principal-component analysis confirmed that secretomes from TxWT-treated cells formed a cluster that was independent from senescence-inducers APH and ETP, and negative controls untreated and TxHQ (Figure 1I).

To identify conserved mediators of paracrine senescence, the secretomes of all senescence inducers (TxWT, APH, and ETP) were filtered against the untreated control (Figure S3F). The TGF-β family member GDF15 was immediately striking (labeled red in Figure 1H), which was also identified in the TxWT-induced secretome (Figure 1H). GDF15 is differentially expressed during aging, negatively regulates IL-6 expression, and was identified as a SASP component promoting colon cancer.[38–40]

To identify constituents specifically enriched in txSASPs, secretome-TxWT was filtered against the secretomes from both negative (Unts, TxHQs) and positive controls (APH, ETP) (Figure S3G). We found regulators of TGF-β signaling INHBA, TGFBR3, FST, the transmembrane protein vasorin (VASN), and metalloprotease ADAM17. However, though significantly up-regulated in secretome-TxWT across all conditions, INHBA (labeled red) was also found up-regulated in secretome-ETP relative to secretome-APH (Figure 1H, right), suggesting a conserved role for INHBA in senescence. In the search for unique SASP constituents in secretome-TxWT, we identified Wnt5a (labeled red in Figure 1H), which was significantly enriched in secretome-TxWT but was not identified in secretome-APH or -ETP (see workflow in Figure S3G). Thus, Wnt5a is an enriched component of txSASPs that also contains INHBA and GDF15. Taken together, the data strongly implicate TGF-β signaling and Wnt5a in a stress secretome from cells undergoing senescence-like responses due to typhoid toxin.

txSASP is orchestrated by ATM and ATR

To understand how a txSASP is established, we validated the presence of INHBA, GDF15, and Wnt5a in senescent cells at 48 h (depicted in Figure 2A). In contrast to the nuclease-deficient TxHQ, treatment with TxWT induced expression of INHBA, GDF15, and Wnt5a, which was coincident with γH2AX (Figures 2B–2F). Previously, typhoid toxin was shown to cause ATM-dependent γH2AX foci that labeled DSBs in the G1 phase of the cell and ATR-dependent Replication Protein A (RPA) foci, which labeled SSBs marked by pan-γH2AX in G2.[23] Thus, ATM and ATR respond to distinct DDRs induced by typhoid toxin. Indeed, the distinct DDRs were observed in Figure S1F where intoxicated cells displaying γH2AX foci (white arrows) lacked phosphorylated RPA (pRPA), while nuclei with pan-γH2AX contained pRPA (blue arrows). To dissect the role of ATM and ATR in the establishment of a txSASP by senescent cells, TxSCs were intoxicated in the presence of small-molecule inhibitors of ATM (iATMs) and ATR (iATRs) before analysis at 48 h. We found that Wnt5a was coincident with TxWT-treated cells containing γH2AX foci (white arrow) and pan-γH2AX (blue arrow) (Figure 2C). Consistent with this, Wnt5a expression was significantly reduced in the presence of iATRs or iATMs and when both inhibitors were applied in combination (Figure 2F). The same trend was observed for GDF15 (Figure 2D). In contrast, only ATR significantly contributed to TxWT-induced expression of INHBA (Figure 2E). We confirmed that cells treated with iATM and iATR cells

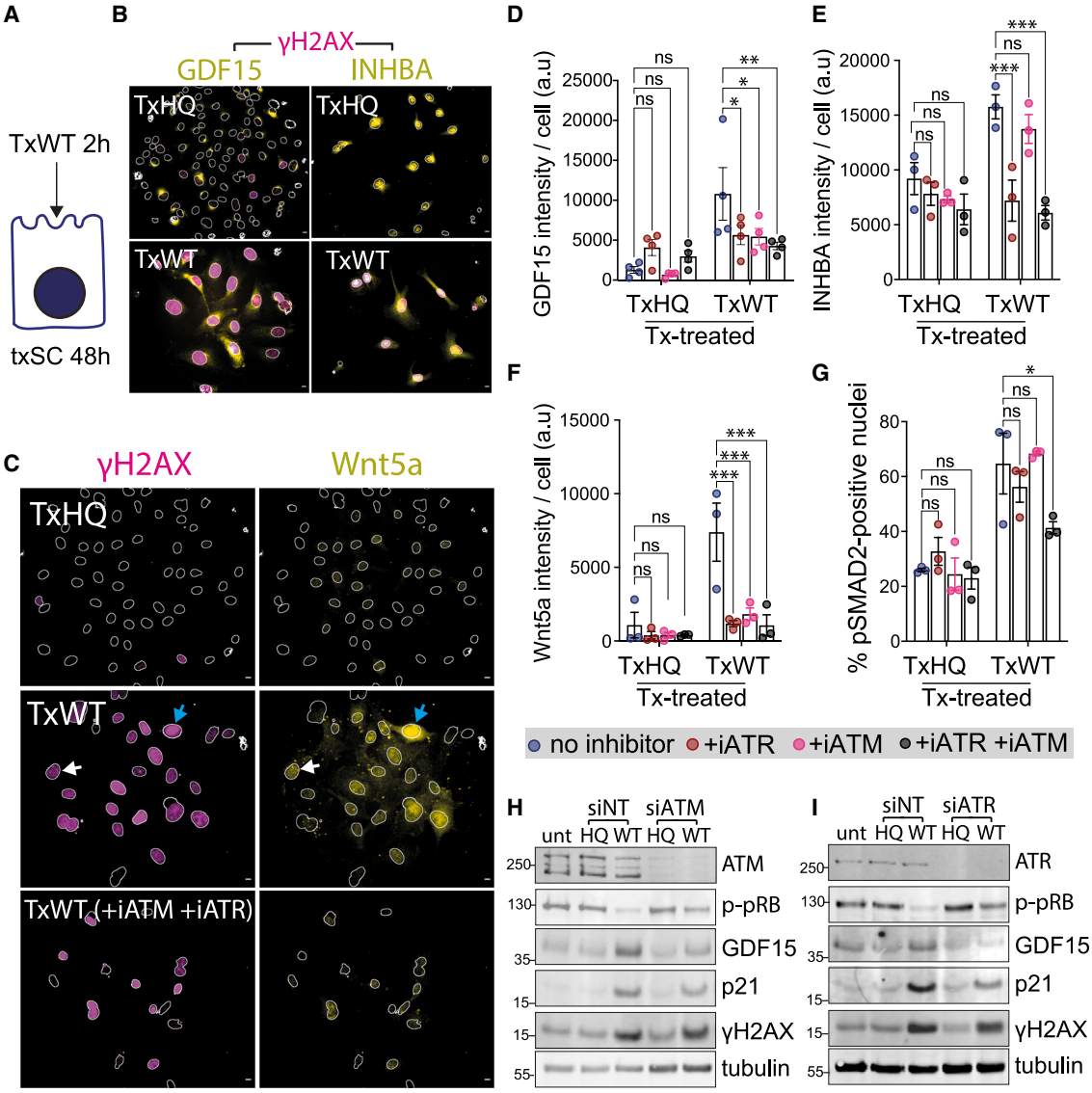

Figure 2. Regulation of txSASP by ATM and ATR

(A) Cartoon depicting TxSCs analyzed at 48 h.

(B) Images of γH2AX (magenta) and GDF15 and INHBA (yellow) in TxWT- or TxHQ-treated cells. Outlines of nuclei indicated.

(C) Same experiment as in (B) assaying Wnt5a expression ± inhibitors of ATM and ATR. Arrows indicate γH2AX foci (white) or pan-γH2AX (blue). Scale bars represent 10 μm.

(D–G) Quantification of (D) GDF15 (n = 4), (E) INHBA (n = 3), and (F) Wnt5a expression (n = 3) or (G) percentage of pSMAD2-positive nuclei (n = 4) in TxWT- or TxHQ-treated cells at 48h ± inhibitors of ATM and ATR. Intensity of GDF15, INHBA, and Wnt5a quantified using Q3, and proportion of pSMAD2-positive nuclei quantified using protocol Q2b.

(H) Immunoblot of TxWT- or TxHQ-treated cells depleted of ATM at 48 h. Cells were intoxicated for 2 h and then immediately transfected with non-targeting (siNT) or ATM (siATM) siRNA for 48 h before immunoblotting. MW in kDa, left.

(I) Immunoblot of TxWT- or TxHQ-treated cells depleted of ATR at 48 h performed as in (H) with siATR.

In (D)–(G), asterisks indicate significance relative to no inhibitor controls calculated by two-way ANOVA with Dunnett's multiple comparisons test. Data represented as mean ± SEM. *p < 0.05, **p < 0.01, ***p < 0.001, ****p < 0.0001, ns denotes non-significance.

See also Figure S4.

were viable, and therefore the reduction in expression of GDF15, INHBA, and Wnt5a was due to their regulation by the DDR kinases (Figure S4A). A role for ATM and ATR was further indicated by immunoblotting experiments (Figures 2H and 2I): HT1080 cells were intoxicated for 2 h and then immediately transfected with non-targeting small interfering RNA (siRNA; siNT) or siRNA targeting ATM (siATM) or ATR (siATR) before immunoblotting at 48 h. ATM and ATR depletion was confirmed in cells

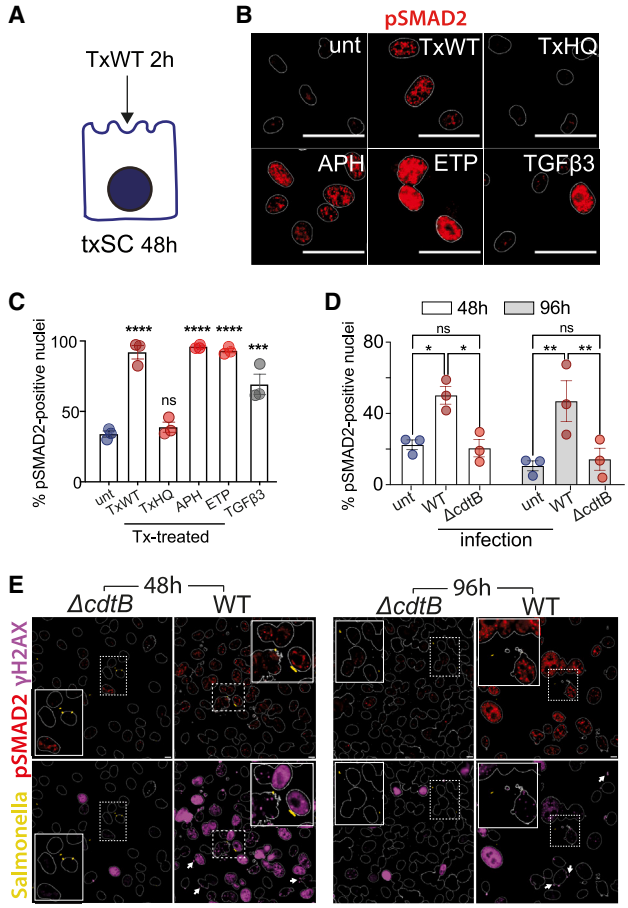

Figure 3. Typhoid toxin activates the TGF-β pathway during *Salmonella* infection

(A) Cartoon depicting TxSCs analyzed at 48 h.

(B) pSMAD2 in cells at 48 h following indicated treatments.

(C) Quantification of (B) relative to untreated cells. Q2a (n = 3).

(D) Quantification of pSMAD2-positive cells at 48 and 96 h following 30 min infection with WT or *ΔcdtB S*. Javiana (MOI: 50). Q2b (n = 3).

(E) Images of (D) showing pSMAD2 (red), γH2AX (magenta), and *Salmonella* (yellow). Magnified insets highlight *Salmonella*. White arrows indicate micronuclei. Outlines of nuclei indicated in (B) and (E).

Scale bars represent 50 μm (B) or 10 μm (E). Significance calculated by (C) one-way ANOVA with Tukey's multiple comparisons test and (D) two-way ANOVA with Sidak multiple comparisons test. Data represented as mean ± SEM. *p < 0.05, **p < 0.01, ***p < 0.001, ****p < 0.0001, ns denotes non-significance.

See also Figure S4.

transfected with siATM or siATR compared with Unts and siNT-transfected cells. In siNT-transfected cells treated with TxHQ, cells were equivalent to untreated cells, and all exhibited *p*-pRb, marking cell-cycle progression. In siNT-transfected cells treated with TxWT, we found γH2AX DDRs and senescence responses marked by p21 and suppression of *p*-pRb, which was coincident with expression of GDF15. In siATM- or siATR-transfected cells, however, TxWT-induced GDF15 and p21, as well as suppression of *p*-pRb, were not observed. γH2AX was still apparent, suggesting redundancy with respect to ATM- and ATR-mediated H2AX phosphorylation. Taken together, the findings indicate a prominent role for ATM and ATR in driving expression of TGF-β ligands and Wnt5a in TxSCs.

S. Javiana activates SMAD2 through nuclease activity of typhoid toxin

Elevated TGF-β signaling has been previously observed in mice infected with *Salmonella* Typhimurium,[41] but no role in the host-pathogen interaction has been ascribed. TGF-β and INHBA activate type 1 ALK tyrosine kinase receptors (ALK1–7) that phosphorylate SMAD2/3 transcription factors, while BMPs tend to activate SMAD1/5/8, both of which drive gene transcription in diverse cellular pathways including senescence.[37] Robust phosphorylation of SMAD2 (pSMAD2) at 48 h was induced in HT1080 fibroblasts by TxWT in a nuclease-dependent manner, as TxHQ was equivalent to untreated controls (Figures 3A–3C). SMAD2 activation was enhanced via ATM and ATR (Figure 2G). TxWT-dependent pSMAD2 signaling was also observed in HIEC6 intestinal epithelial cells and IMR90 and NIH3T3 fibroblasts (Figures S4B–S4D). TGF-β ligands were observed to be secreted in response to TxWT, APH, and ETP at 48 h (Figures 1H and S3F). Consistent with a conserved role for TGF-β ligands in paracrine senescence and their secretion in response to APH and ETP (Figures 1H and S3F), APH and ETP triggered pSMAD2 production, which was also observed with the positive control TGF-β3 at 48 h (Figures 3B and 3C). The same trend was observed in SMAD1/5, which was activated by TxWT, APH, and ETP, but not TxHQ, at 48 h (Figures S4E and S4F). *S.* Javiana has been shown to elicit cell death and senescence responses during infection in a toxin-dependent manner.[23,26,42] We found that infection of host cells by WT toxigenic *S.* Javiana induced widespread γH2AX, which was coincident with activation of SMAD2 that was evident in ~50% of cells at 48 h, indicating cellular senescence (Figures 3D and 3E). No differences in SMAD2 activation were observed between untreated and *ΔcdtB S*. Javiana, confirming a requirement for typhoid toxin. Relative to recombinant TxWT, we reasoned that there would be a delay in the toxigenic effects of *S.* Javiana due to the time needed to express and exocytose typhoid toxin from the host cell.[21] We accounted for the delay by imaging infected cells at 96 h, at which point pSMAD2 had intensified (exemplified by Figure 3E), though when quantified, the proportion of pSMAD2-positive cells remained at ~50% (Figure 3D). In addition, WT, but not *ΔcdtB*, *S*. Javiana induced formation of γH2AX-label\ed micronuclei (Figure 3E, white arrows), a marker of genotoxicity,[43] which was not consistently observed with recombinant TxWT (Figure S1F). In summary, the data show that typhoid toxin activates SMAD transcription factors, which are known to be downstream of TGF-β-family ligands identified in secretome-TxWT.

Crosstalk between Wnt5a and TGF-β ligands enforces DDRs and senescence responses

We next sought to determine the contribution of GDF15, INHBA, and Wnt5a to the TxSC phenotype as depicted in Figure 4A. HT1080 cells were intoxicated for 2 h prior to transfection with SMARTpools of siNT, siGDF15, siINHBA, siSMAD2, and siWNT5A and immunoblotting at 48 h with indicated antibodies, which confirmed protein depletion in each case (Figure 4B). In siNT control cells, TxWT, but not TxHQ, induced senescence

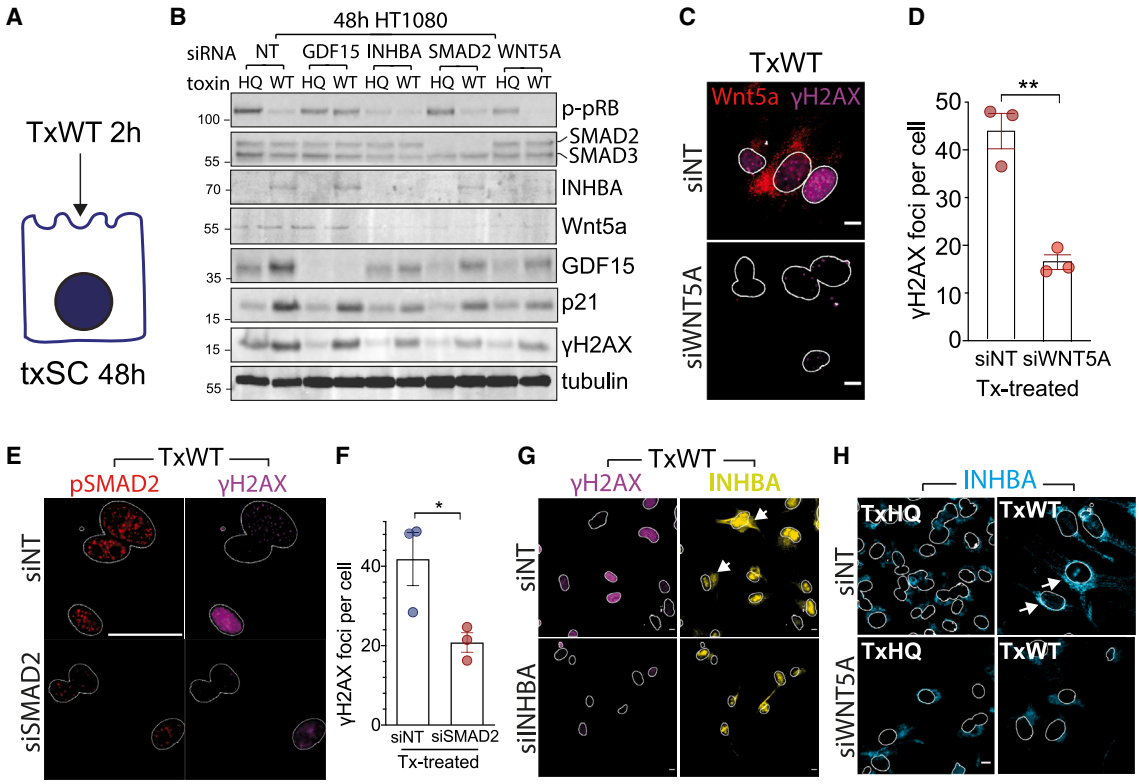

Figure 4. Toxin induction of Wnt5a and TGF-β-mediated host DDR and senescence

(A) Cartoon depicting TxSCs analyzed at 48h.

(B) Immunoblot of cells treated for 2 h with TxHQs or TxWT and then transfected with NT, GDF15, INHBA, SMAD2, or WNT5A siRNAs before immunoblotting at 48 h with indicated antibodies. MW in kDa, left.

(C) Images of Wnt5a (red), γH2AX (magenta), and DAPI (outlines) in TxWT-treated siNT- or siWNT5A-transfected cells at 48 h.

(D) Quantification of γH2AX foci per nucleus from experiment in (C). Q4 (n = 3).

(E) Images of pSMAD2 (red), γH2AX (magenta), and DAPI (outlines) in TxWT-treated siNT- or siSMAD2-transfected cells at 48 h.

(F) Quantification of γH2AX foci per nucleus from experiment in (E). Q4 (n = 3).

(G) Images of INHBA (yellow), γH2AX (magenta), and DAPI (outlines) in TxWT-treated siNT- or siINHBA-transfected cells at 48 h.

(H) Images of INHBA (cyan) and DAPI (outlines) in TxWT- or TxHQ-treated cells transfected with siNT or siWNT5A for 48 h.

(G and H) Arrows indicate increased INHBA. In (D) and (F), significance calculated by unpaired t test. Data represented as mean ± SEM. *p < 0.05, **p < 0.01, ***p < 0.001, ****p < 0.0001, ns denotes non-significance. Scale bars represent 10 μm (C, G, and H) and 50 μm (E).

See also Figure S5.

responses marked by γH2AX, p21 expression, and suppression of *p*-pRb, which was coincident with increased expression of txSASP factors GDF15, INHBA, and, to a lesser extent, Wnt5a.

Relative to siNT-transfected cells, we found that siGDF15 increased *p*-pRb but had no effect on γH2AX and p21 or on secretome components INHBA and Wnt5a. Thus, while GDF15 can track toxin-induced senescence, it appears to have no clear role in establishing TxSCs or txSASP factors. This was not the case for INHBA, SMAD2, and Wnt5a, whose depletion by siRNA transfection reduced toxin-induced γH2AX DDRs, p21, and GDF15 (Figure 4B). The reduction in γH2AX DDRs was also observed by fluorescence microscopy in TxSCs transfected with siINHBA, siSMAD2, and siWNT5A SMARTpools (Figures 4C–4G). When we further examined Figure 4B, we found evidence of regulatory interplay between txSASP factors and the TGF-β pathway since INHBA, SMAD2, and Wnt5a each enhanced expression of GDF15. Moreover, INHBA mediated expression of Wnt5a, and vice versa. Further synergy was indicated by a role for SMAD2 in the expression of Wnt5a. The same trends were observed with single siRNAs targeting INHBA, SMAD2, or Wnt5a, which also reduced γH2AX, and senescence markers p21 and GDF15 in TxSCs (Figures S5A–S5C).

We focused on Wnt5a, which was found as a unique SASP constituent of secretome-TxWT (Figure 1H). Quantification of immunoblots found that siWNT5A significantly reduced GDF15 and INHBA in TxSCs (Figures S5D and S5E), which was further supported by fluorescence microscopy, indicating that GDF15 and INHBA expression was driven by Wnt5a (white arrows in Figures 4H, S5G, and S5H). Distinct INHBA antibodies further substantiated Wnt5a-mediated INHBA expression in TxSCs (Figures 4H and S5H). Quantification of immunoblots also showed that siWNT5A significantly reduced p21 expression in TxSCs (Figure S5F). However, p21 was still significant

relative to TxHQ-treated control cells, indicating that Wnt5a promotes, but is not sufficient for, senescence responses. Indeed, siWNT5A-transfected TxSCs still exhibited SA-β-Gal (Figures S5I and S5J). Thus, Wnt5a likely plays an additive role by exacerbating effects of TxWT-induced DNA breaks. Taken together, the findings show that DDRs induced by the nuclease activity of typhoid toxin are enforced by INHBA and Wnt5a, which affect TGF-β pathway regulation during host senescence.

Toxin-induced Wnt5a and INHBA establish paracrine senescence

The observation that INHBA and Wnt5a enhanced DDRs in TxSCs suggests that INHBA and Wnt5a either synergize with the toxin directly (e.g., as co-factors for toxin nuclease activity) or induce DDRs independently in TxSCs. If the latter were true, then we reasoned that INHBA and Wnt5a may directly underlie toxin-induced paracrine senescence in naive cells, a characteristic of txSASPs (depicted in Figure 5A). Thus, we applied secretome-TxWT to naive HT1080 cells in the presence or absence of neutralizing INHBA and/or Wnt5a antibodies before analyzing paracrine senescence through EdU labeling at 120 h (Figures 5B and 5C). Indeed, paracrine senescence by secretome-TxWT was significantly impaired in the presence of neutralizing INHBA or Wnt5a antibodies (Figure 5C). No additive effect was observed when INHBA and Wnt5a antibodies were used in combination, suggesting that they mediate paracrine senescence via the same pathway (Figures 5B and 5C). In support of this view, we observed paracrine senescence with purified INHBA and Wnt5a, which was significantly enhanced when the ligands were combined in secretome-TxHQs (Figure S6A). This was coincident with pSMAD2 (Figures S6B and S6C), which has been previously reported in a INHBA- and Wnt5a-dependent manner.[37,44] Moreover, neutralizing INHBA and Wnt5a antibodies impeded SMAD2 activation, which indicated specificity against INHBA and Wnt5a (Figures S6B and S6C).

To further investigate Wnt5a, we transfected cells with siWNT5A for 48 h prior to intoxication with TxWT. Imaging 48 h post-intoxication confirmed Wnt5a depletion (Figures S5I and S5J), and the resulting Wnt5a-depleted secretome-TxWT was used for assaying paracrine senescence in naive HT1080 cells at 120 h (Figures 5D–5F). The secretome-TxWT from control siNT-transfected TxSCs induced paracrine senescence in naive cells (Figures 5D–5F). Relative to secretome-TxWT from siNT cells, the paracrine senescence was significantly impaired by Wnt5a-depleted secretomes harvested from TxSCs transfected with both SMARTpools or single siRNAs targeting Wnt5a (Figures 5E and 5F). No difference was observed when the same experiment was performed with TxHQs. Consistent with Wnt5a directly regulating the TGF-β pathway (Figures 4B and S5A), Wnt5a-driven paracrine senescence by secretome-TxWT was coincident with activation of SMAD2 in naive cells (Figures 5E and 5G). Moreover, a small-molecule inhibitor of ALK receptors 4, 5, and 7 impeded the ability of secretome-TxWT to induce paracrine senescence (Figures S6E–S6G). In summary, once deployed from TxSCs, INHBA and Wnt5a act in synergy and are sufficient to mediate paracrine senescence.

Wnt5a and GDF15 enhance *Salmonella* invasion of human host cells

Salmonella invades cells by promoting host cytoskeleton remodeling.[45] Typhoid toxin is not directly involved in *Salmonella* invasion, as it is expressed intracellularly from 3 h,[21,28] yet txSASP was previously shown to promote *Salmonella* invasion into macrophages through unidentified factors in secretome-TxWT.[23] Thus, we sought to address the role of Wnt5a in invasion by infecting cells for 30 min with *ΔcdtB S.* Javiana, which bypassed a possible contribution from typhoid toxin. We found that supplementing fresh growth media with purified Wnt5a enhanced *Salmonella* uptake into human macrophages (Figure 5H). Though GDF15 played little part in establishing TxSCs (Figure 4B), we speculated that its secretion from TxSCs might influence infection of bystander cells, which would identify a role for GDF15 in txSASPs. In support of this view, purified GDF15 induced a modest but significant increase in *Salmonella* invasion (Figure 5I). Purified GDF15 elicited SMAD2 activation, which was blocked by neutralizing GDF15 antibodies, confirming specificity (Figure S6D). We found that secretome-TxWT, but not secretome-TxHQs, enhanced *Salmonella* infection of macrophages, which was impeded by neutralizing GDF15 and Wnt5a antibodies (Figure 5J). When both GDF15 and Wnt5a antibodies were used in combination, there was no additive effect, indicating that GDF15 and Wnt5a promote phagocytosis. We also found that secretome-TxWT, but not secretome-TxHQs, enhanced *Salmonella* invasion into fibroblasts, further indicating that toxin-induced senescence increases virulence (Figure S6H). Therefore, the typhoid toxin mediates expression of GDF15 through Wnt5a that both promote intracellular *Salmonella* infections.

Wnt5a is required for survival of intestinal cells undergoing toxin-induced senescence

We next investigated Wnt5a in human intestinal cells, which are a target host cell of toxigenic *Salmonella*. As depicted in Figure 6A, we intoxicated HCT116 intestinal cells for 2 h with TxWT or TxHQs before assessing TxSC responses at 48 h by immunoblotting (Figures 6B and S7A). In untreated and TxHQ-treated control cells, no DDRs were observed, and *p*-pRb indicated proliferation. In TxWT-treated cells, suppression of *p*-pRb marked cell-cycle arrest in a dose-dependent manner. Cell-cycle arrest coincided with toxin-induced γH2AX, p21 expression, GDF15 and Wnt5a, with the latter at the limit of detection at 48 h (Figure 6B). HCT116 cells have previously been used to study senescence responses to ETP at 168 h.[46] When we extended TxWT treatment to 168 h, we found that the relative expression of txSASP factors GDF15 and Wnt5a had further increased, while γH2AX and p21 persisted, albeit at a reduced level. In negative control cells, *p*-pRb had diminished, which was likely due to quiescence, as senescence markers were of low expression, if expressed at all. In agreement with expression of txSASP factor Wnt5a at 168 h, we found that the harvested secretome-TxWT induced paracrine senescence in naive HCT116 cells (Figures S6I, S6J, and S6K).

As an additional control, we treated HCT116 intestinal cells with typhoid toxin containing an S35A mutation in PltB (TxSA), which has been shown to impair cell surface receptor binding and therefore toxin uptake.[22,47] Relative to TxWT, we found that the S35A mutation in TxSA attenuated γH2AX DDRs, p21

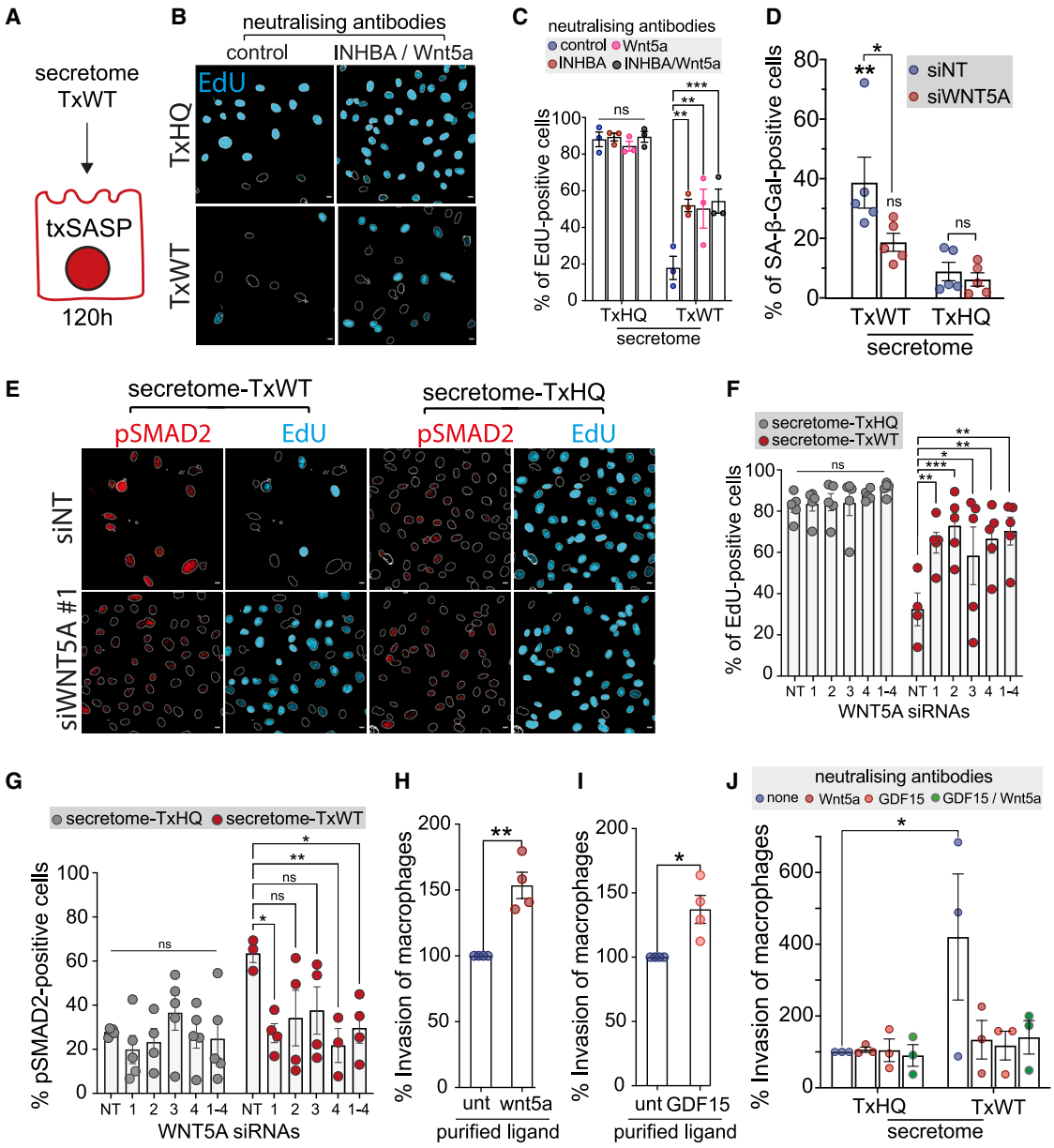

Figure 5. Paracrine senescence by Wnt5a and INHBA

(A) Experimental schematic.

(B) Replicating (blue: EdU-positive) and cell-cycle-arrested (EdU-negative) HT1080 cells treated for 120 h with secretome-TxHQ or secretome-TxWT in the presence or absence of neutralizing Wnt5a and INHBA antibodies. DAPI outlines shown. Scale bars represent 10 μm.

(C) Quantification of experiment in (B). Q1 (n = 3).

(D) Quantification of paracrine SA-β-Gal in naive HT1080 cells treated for 120 h with Wnt5a-depleted secretome-TxWT or secretome-TxHQs. Secretomes were harvested from HT1080 cells transfected for 48 h with siNT or SMARTpool siWNT5A before 48 h intoxication with TxWT or TxHQs. Wnt5a-depleted secretomes were incubated with naive HT1080 cells for 120 h before quantifying SA-β-Gal. Q6 (n = 5).

(E) Naive HT1080 cells treated for 120 h with Wnt5a-depleted secretome-TxWT or secretome-TxHQs as in (D) using WNT5A siRNA #1 prior to immunofluorescence of pSMAD2 (red), EdU (blue), and DAPI (outlines). Scale bars represent 10 μm.

(F and G) Quantification of replicating EdU-positive cells in (F) using Q1 (n = 4–5) and pSMAD2-positive nuclei in (G) using Q2b (n = 3–5) from experiment in (E).

(H–J) Quantification of *Salmonella* invasion into THP1 macrophages following a 30 min infection with *ΔcdtB S.* Javiana (MOI: 20) added to cells at the same time as (H) 0.05 μg/mL purified Wnt5a (n = 4), (I) 0.2 μg/mL GDF15 (n = 4), or (J) secretome-TxWT or secretome-TxHQs with or without neutralizing Wnt5a and GDF15 antibodies (n = 3). Invasion quantified by counting colony-forming units following 1.5 h incubation in gentamicin-containing media.

Significance calculated by two-way ANOVA with (C and G) Dunnett's, (D) Tukey's, and (F and J) Sidak multiple comparisons tests and (H and I) unpaired t test. Data represented as mean ± SEM. *p < 0.05, **p < 0.01, ***p < 0.001, ****p < 0.0001, ns denotes non-significance.

See also Figure S6.

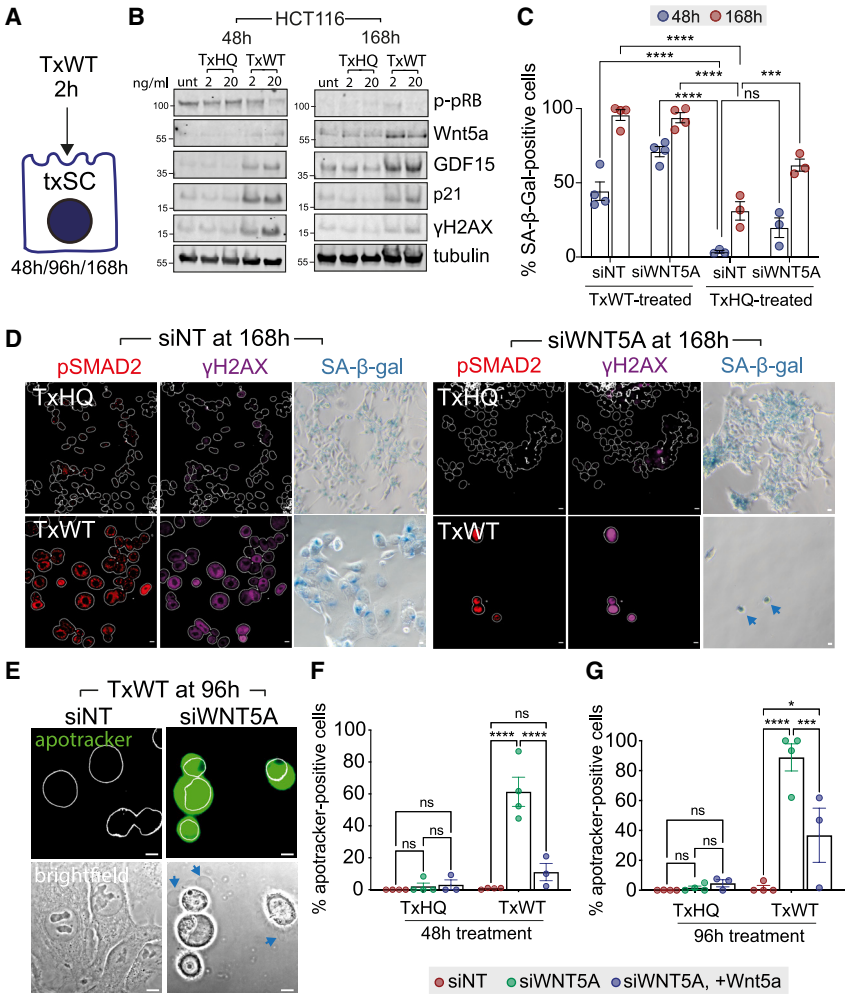

Figure 6. Wnt5a-dependent toxin-induced senescence in HCT116 intestinal cells

(A) Cartoon depicting TxSCs analyzed at 48, 96, or 168 h.

(B) Immunoblot of HCT116 cells either untreated (unt) or treated with indicated concentrations of TxHQs or TxWT for 2 h before analysis at 48 and 168 h.

(C) Quantification of SA-β-Gal-positive HCT116 cells treated with TxHQs or TxWT for 2 h before transfection with siNT or siWNT5A and analysis at either 48 or 168 h. Q6 (n = 3–4).

(D) Images of the experiment in (C) showing fluorescence microscopy of pSMAD2 (red), γH2AX (magenta), and DAPI (outlines) or bright-field microscopy of SA-β-Gal (blue) at 168 h. Blue arrows indicate SA-β-Gal-positive siWNT5A-transfected cells. Scale bars represent 10 μm.

(E) HCT116 cells treated with TxWT for 2 h before transfection with siNT or siWNT5A for 96 h and then labeled with Apotracker (green) and DAPI (outlines) (top) and the same cells with bright-field light microscopy (bottom). Blue arrows indicate blebbing. Scale bars represent 10 μm.

(F) Quantification of apoptotic cells at 48 h. HCT116 cells treated with TxWT or TxHQs for 2 h before transfection with siNT or siWNT5A in the presence or absence of purified Wnt5a (0.5 μg/mL) and labeling with Apotracker at 48 h (n = 3–4). Q5.

(G) Quantification of apoptotic cells as in (F) at 96 h (n = 3–4).

Significance calculated using two-way ANOVA with multiple comparisons tests: (C) Dunnett's, (F) Sidak, and (G) Tukey's. Data represented as mean ± SEM. *p < 0.05, **p < 0.01, ***p < 0.001, ****p < 0.0001, ns denotes non-significance.

See also Figures S6 and S7.

and GDF15 expression at 48 h in a dose-dependent manner (Figures S7A and S7B), while SA-β-Gal was impaired at 168 h (Figure S7C). Thus, the PltB residue S35, important for toxin uptake, is also important for mediating toxin-induced senescence.

The findings in Figure 6B suggest that characteristics of senescence were adopted at 48 h and became more established over 168 h. Indeed, TxWT-induced SA-β-Gal was apparent in ~25% of cells at 48 h, which increased to ~75% by 168 h (Figures S7D–S7F). The relative increase in SA-β-Gal observed with TxWT at 48 h and 168 h was also observed with positive controls ETP and APH, but not negative controls TxHQ and untreated (Figure S7E).

We next addressed the role of Wnt5a in intestinal TxSC responses. HCT116 cells were treated with TxWT for 2 h prior to siWNT5A transfection before analysis by immunoblotting (Figure S7G). Wnt5a depletion in TxSCs impaired senescence responses including GDF15 expression and, to a lesser extent, p21 and γH2AX (Figure S7H). This was also observed with siINHBA and siSMAD2 but not siGDF15, mirroring the trend in HT1080 fibroblasts. Taken together, the findings show that the synergy between Wnt5a and TGF-β ligands is conserved across cell types during TxSC responses.

When we investigated Wnt5a-depleted cells at 48 and 168 h by microscopy, we observed no differences in pSMAD2, indicating that additional factors in secretome-TxWT of HCT116 cells contribute to TGF-β signaling (Figures 6D and S7H). The proportion of cells exhibiting SA-β-Gal too was unaffected by siWNT5A (Figure 6C), as was also observed in Wnt5a-depleted HT1080 cells (Figure S5I). However, locating Wnt5a-depleted SA-β-Gal-positive TxSCs for image analysis at 168 h proved remarkably difficult due to a marked reduction in the number of intestinal TxSCs (Figure 6D, blue arrows) indicative of cell death. This was not the case for SMAD2-depleted TxSCs (Figure S7I), which persisted as cell-cycle-arrested senescent cells that further indicated a SMAD2-independent role for Wnt5a during senescence in HCT116 cells. To investigate the loss of TxSCs, we imaged Wnt5a-depleted TxSCs at 48 and 96 h in the presence of the fluorescent probe Apotracker, which identifies apoptotic cells (Figures 6E–6G). To increase the likelihood of capturing cells for image analysis, the time points were reduced from 168 to 96 h. In siNT control cells, Apotracker was absent from TxWT-treated cells. However, Wnt5a-depleted TxSCs were labeled with Apotracker and displayed extensive cell

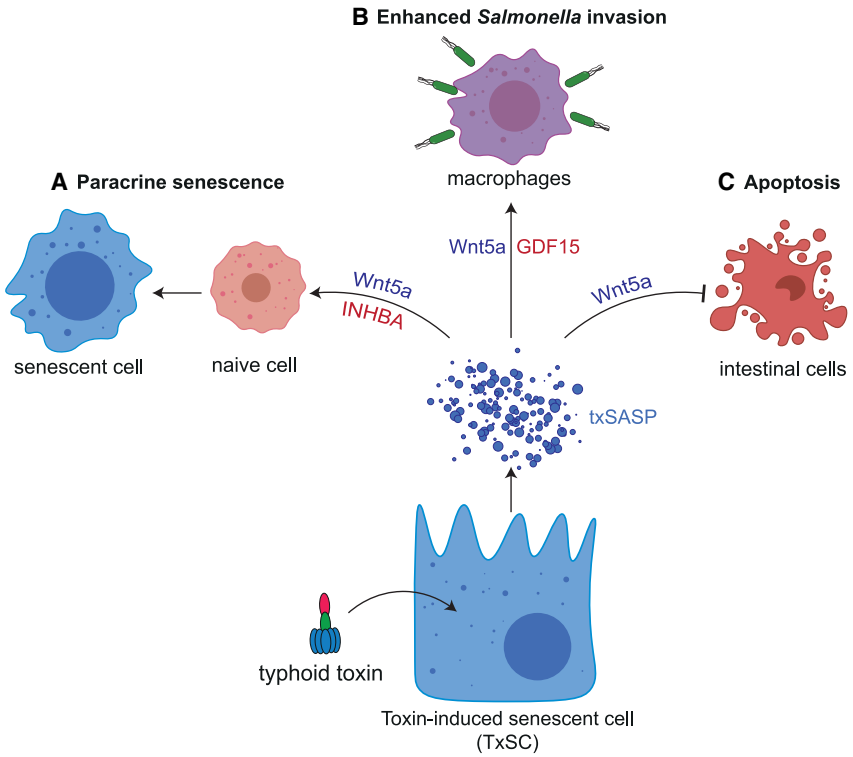

Figure 7. Model showing Wnt5a-mediated senescent responses through typhoid toxin

TxSCs secrete Wnt5a, which augments expression of INHBA and GDF15, which are also secreted in the host secretome-defining txSASP.

(A) Wnt5a synergizes with INHBA to mediate paracrine senescence.

(B) Wnt5a synergizes with GDF15 to promote *Salmonella* invasion.

(C) Wnt5a is required for resisting apoptosis in intestinal epithelial cells, thereby facilitating establishment of TxSCs.

rounding and surface blebbing under bright-field light microscopy (blue arrows), which are defining features of apoptosis.[48] In contrast, siNT control TxSCs exhibited the typical flattened morphology of senescent cells (Figure 6E). To control for off-target effects by siWNT5A, we supplemented siWNT5A-transfected TxWT-treated cells with purified Wnt5a (+Wnt5a) at the time of siRNA transfection (Figures 6F and 6G). This counteracted apoptosis and significantly rescued Wnt5a-depleted TxSCs, which enabled the establishment of Wnt5a-dependent senescence in response to typhoid toxin.

DISCUSSION

A SASP is considered a double-edged sword capable of exerting the beneficial effects of senescence (e.g., tumor suppression) or its deleterious effects (e.g., cancer progression, aging).[7,8] To limit proliferation of cancer or virus-infected cells, SASP factors can reinforce and spread senescence in autocrine and paracrine mechanisms, thereby providing a powerful defense.[7,8,13–15] However, bacterial pathogens are not reliant on mammalian DNA replication machinery for proliferation, and the SASP consequently provides a possible hijack target during infection. Here, we resolved the identity of a host secretome released in response to genotoxic stress from typhoid toxin, which resulted in paracrine senescence and enhanced infections through Wnt5a and its potentiation of the TGF-β pathway (Figure 7).

A role for TGF-β in senescence induced by bacterial pathogens has not been previously described. Consistent with this role, SMAD2/3 activation by TGF-β ligands induces cell-cycle arrest by repressing proliferation factors while increasing expression of CDK inhibitors.[49] We found that toxin-driven expression of TGF-β ligands INHBA, SMAD2, and Wnt5a augmented expression of the CDK inhibitor p21 in TxSCs. TGF-β signaling also induces reactive oxygen species and DNA damage.[49] Indeed, we found that Wnt5a, SMAD2, and INHBA amplified γH2AX DDRs in TxSCs, previously observed with INHBA during oncogene-induced senescence.[12,50,51] Besides autocrine effects on TxSCs, we found that INHBA and Wnt5a mediated paracrine senescence in naive cells. Thus, INHBA and Wnt5a play dual roles in senescence responses to typhoid toxin: (1) enforcing senescence in TxSCs through p21- and γH2AX-labeled DDRs and (2) perpetuating senescence to bystander cells through paracrine effects (Figure 7A). We also found that Wnt5a and INHBA drove their respective expression, indicating positive feedback. Thus, our findings suggest that Wnt5a mediates expression of INHBA, which causes paracrine senescence involving the SMAD2/3-dependent TGF-β pathway. In support of this mechanism, Wnt5a has been shown to potentiate the activity of TGF-β1 during regeneration of damaged colonic crypts in mice.[52] This study consequently expands the synergistic role of Wnt5a and TGF-β to pathogen-induced senescence responses.

We found that Wnt5a was only required for establishing senescence in intestinal cells, where the loss of Wnt5a caused apoptosis in response to typhoid toxin (Figure 7C). A hallmark of senescence is resistance to cell death.[8] Though Wnt5a has not been shown to enforce survival of senescent cells before, *Salmonella* appears to evade apoptosis by hijacking Wnt5a, which acts through an unknown mechanism. Unlike Wnt5a, SMAD2 played no role in the survival of TxSCs. Though Wnt5a may act through SMAD1/5 of the TGF-β pathway, Wnt5a suppresses apoptosis through effectors Wnt1-inducible secreted protein-1, β-catenin, ERK, and AKT,[53–56] any of which may enable typhoid toxin to establish senescent intestinal cells. Thus, Wnt5a has divergent cell-type-dependent roles in senescence by mediating evasion of apoptosis in intestinal cells and not fibroblast cells.

The human host secretome plays a critical part in determining the outcome of bacterial infections. For example, the *Salmonella* effector SlfA diverts antimicrobial cargo for exocytosis, thereby

promoting intracellular survival of *Salmonella*.[30] On the other hand, host secretion can counteract infections: toxin inactivation of Rho GTPases is sensed by host inflammasomes, resulting in secretion of IL-1β and IL-18, which recruit immune cells.[32] Here, we identify Wnt5a and GDF15 as secreted txSASP factors that enhance *Salmonella* infection (Figure 7B). Bacterial hijacking of GDF15 and WNT5a has not been previously observed. Wnt5a has been shown to promote phagocytosis of *Escherichia coli*,[57] as well as *Streptococcus pneumoniae* and *Pseudomonas aeruginosa*, where Wnt5a was also implicated in bacterial clearance.[58] Thus, Wnt5a can act in host defense. However, *Salmonella* survives within macrophages and is thus able to hijack Wnt5a for invasion through a toxin-induced host secretome.

Salmonella exploits chronic senescence in aging organisms, indirectly, during colonization of systemic sites,[59] chronic *Salmonella* carriage,[60] and pathogen entry into senescent fibroblasts from elderly volunteers.[61] This is consistent with the view that senescence increases susceptibility to infection in aging organisms.[7] Our findings indicate that *Salmonella* employs typhoid toxin to directly accelerate aging-like responses through acute senescence, which may be significant *in vivo.* During infection of mice, *Salmonella* elicits senescence in a toxin-dependent manner that suppresses inflammatory responses.[24,29] This is consistent with up-regulation of TGF-β ligands in txSASPs and down-regulation of IL-6, which is an inflammatory mediator of SASPs.[8] Similarly, oncogene-induced SASPs enriched in TGF-β1/3 suppressed immunosurveillance of cancer cells.[8,14] Thus, our study advances the senescence field through an emerging theme investigating acute senescence responses to pathogenic bacteria. We revealed a *Salmonella* hijack mechanism dependent on Wnt5a and its potentiation of the TGF-β pathway. The findings are of significance to those studying the interplay between innate immunity and senescence and those investigating how bacterial pathogens exploit host DDRs to cause disease.

Limitations of the study

This study uses HT1080 and HCT116 cancer cell lines that express senescence markers such as p21 but lack others such as p16.[62] Despite identifying the same txSASP factors in different cell types, signaling mechanisms may deviate from *Salmonella*-infected humans. This is perhaps unsurprising, as SASP composition varies depending on the senescence inducer, duration, microenvironment, and cell type.[8] It will be important to determine whether typhoid toxin induces a host secretory phenotype in humans during typhoid fever or related diseases caused by *Salmonella*.

STAR★METHODS

Detailed methods are provided in the online version of this paper and include the following:

- KEY RESOURCES TABLE
- RESOURCE AVAILABILITY
  - Lead contact
  - Materials availability
  - Data and code availability
- EXPERIMENTAL MODEL AND SUBJECT PARTICIPANT DETAILS
  - Cell lines and maintenance
  - *Salmonella* strains
- METHOD DETAILS
  - Toxin purification and intoxication
  - Cell culture treatments
  - siRNA transfection
  - *Salmonella* infection
  - Immunoblotting
  - Immunofluorescence
  - Senescence assays
  - Survival assays
  - Secretome harvest and paracrine senescence
  - GeneChip microarray
  - Mass spectrometry-based proteomics
- QUANTIFICATION AND STATISTICAL ANALYSIS
  - Analysis of proteomic data
  - Quantification
  - Image processing
  - Statistics

SUPPLEMENTAL INFORMATION

Supplemental information can be found online at https://doi.org/10.1016/j.celrep.2023.113181.

ACKNOWLEDGMENTS

The research was funded by a UKRI Future Leaders Fellowship to D.H. (MR/S034390/1). We would like to thank Dr. Salma Srour for support and assistance and Dr. Kai Erdmann, Prof. Sherif ElKhamisy and Prof. Martin Wiedmann for reagents. Microscopy was performed at the Wolfson Light Microscopy Facility (MR/K015753/1).

AUTHOR CONTRIBUTIONS

D.H. supervised the study. M.E. and D.H. devised the concept. M.E., M.O.C., and A.E.M.I. performed experiments. All authors designed experiments and analyzed the data. D.H. and M.E. wrote the manuscript.

DECLARATION OF INTERESTS

The authors declare no competing interests.

Received: October 18, 2022
Revised: June 15, 2023
Accepted: September 13, 2023

REFERENCES

1. Polo, S.E., and Jackson, S.P. (2011). Dynamics of DNA damage response proteins at DNA breaks: a focus on protein modifications. Genes Dev. *25*, 409–433. https://doi.org/10.1101/gad.2021311.
2. Burma, S., Chen, B.P., Murphy, M., Kurimasa, A., and Chen, D.J. (2001). ATM phosphorylates histone H2AX in response to DNA double-strand breaks. J. Biol. Chem. *276*, 42462–42467. https://doi.org/10.1074/jbc.C100466200.
3. Ward, I.M., and Chen, J. (2001). Histone H2AX is phosphorylated in an ATR-dependent manner in response to replicational stress. J. Biol. Chem. *276*, 47759–47762. https://doi.org/10.1074/jbc.C100569200.

4. Celeste, A., Fernandez-Capetillo, O., Kruhlak, M.J., Pilch, D.R., Staudt, D.W., Lee, A., Bonner, R.F., Bonner, W.M., and Nussenzweig, A. (2003). Histone H2AX phosphorylation is dispensable for the initial recognition of DNA breaks. Nat. Cell Biol. *5*, 675–679. https://doi.org/10.1038/ncb1004.

5. Yuan, J., Adamski, R., and Chen, J. (2010). Focus on histone variant H2AX: to be or not to be. FEBS Lett. *584*, 3717–3724. https://doi.org/10.1016/j.febslet.2010.05.021.

6. Hernandez-Segura, A., Nehme, J., and Demaria, M. (2018). Hallmarks of Cellular Senescence. Trends Cell Biol. *28*, 436–453. https://doi.org/10.1016/j.tcb.2018.02.001.

7. Humphreys, D., ElGhazaly, M., and Frisan, T. (2020). Senescence and Host-Pathogen Interactions. Cells *9*, 1747, Cells-Basel. https://doi.org/10.3390/cells9071747.

8. Kumari, R., and Jat, P. (2021). Mechanisms of Cellular Senescence: Cell Cycle Arrest and Senescence Associated Secretory Phenotype. Front. Cell Dev. Biol. *9*, 645593. https://doi.org/10.3389/fcell.2021.645593.

9. Coppé, J.P., Patil, C.K., Rodier, F., Sun, Y., Muñoz, D.P., Goldstein, J., Nelson, P.S., Desprez, P.Y., and Campisi, J. (2008). Senescence-associated secretory phenotypes reveal cell-nonautonomous functions of oncogenic RAS and the p53 tumor suppressor. PLoS Biol. *6*, 2853–2868. https://doi.org/10.1371/journal.pbio.0060301.

10. Malaquin, N., Martinez, A., and Rodier, F. (2016). Keeping the senescence secretome under control: Molecular reins on the senescence-associated secretory phenotype. Exp. Gerontol. *82*, 39–49. https://doi.org/10.1016/j.exger.2016.05.010.

11. Acosta, J.C., O'Loghlen, A., Banito, A., Guijarro, M.V., Augert, A., Raguz, S., Fumagalli, M., Da Costa, M., Brown, C., Popov, N., et al. (2008). Chemokine signaling via the CXCR2 receptor reinforces senescence. Cell *133*, 1006–1018. https://doi.org/10.1016/j.cell.2008.03.038.

12. Acosta, J.C., Banito, A., Wuestefeld, T., Georgilis, A., Janich, P., Morton, J.P., Athineos, D., Kang, T.W., Lasitschka, F., Andrulis, M., et al. (2013). A complex secretory program orchestrated by the inflammasome controls paracrine senescence. Nat. Cell Biol. *15*, 978–990. https://doi.org/10.1038/ncb2784.

13. Kang, T.W., Yevsa, T., Woller, N., Hoenicke, L., Wuestefeld, T., Dauch, D., Hohmeyer, A., Gereke, M., Rudalska, R., Potapova, A., et al. (2011). Senescence surveillance of pre-malignant hepatocytes limits liver cancer development. Nature *479*, 547–551. https://doi.org/10.1038/nature10599.

14. Hoare, M., Ito, Y., Kang, T.W., Weekes, M.P., Matheson, N.J., Patten, D.A., Shetty, S., Parry, A.J., Menon, S., Salama, R., et al. (2016). NOTCH1 mediates a switch between two distinct secretomes during senescence. Nat. Cell Biol. *18*, 979–992. https://doi.org/10.1038/ncb3397.

15. Sturmlechner, I., Zhang, C., Sine, C.C., van Deursen, E.J., Jeganathan, K.B., Hamada, N., Grasic, J., Friedman, D., Stutchman, J.T., Can, I., et al. (2021). p21 produces a bioactive secretome that places stressed cells under immunosurveillance. Science *374*, eabb3420. https://doi.org/10.1126/science.abb3420.

16. Cougnoux, A., Dalmasso, G., Martinez, R., Buc, E., Delmas, J., Gibold, L., Sauvanet, P., Darcha, C., Déchelotte, P., Bonnet, M., et al. (2014). Bacterial genotoxin colibactin promotes colon tumour growth by inducing a senescence-associated secretory phenotype. Gut *63*, 1932–1942. https://doi.org/10.1136/gutjnl-2013-305257.

17. González, E., Rother, M., Kerr, M.C., Al-Zeer, M.A., Abu-Lubad, M., Kessler, M., Brinkmann, V., Loewer, A., and Meyer, T.F. (2014). Chlamydia infection depends on a functional MDM2-p53 axis. Nat. Commun. *5*, 5201. https://doi.org/10.1038/ncomms6201.

18. Siegl, C., Prusty, B.K., Karunakaran, K., Wischhusen, J., and Rudel, T. (2014). Tumor suppressor p53 alters host cell metabolism to limit Chlamydia trachomatis infection. Cell Rep. *9*, 918–929. https://doi.org/10.1016/j.celrep.2014.10.004.

19. Siegl, C., and Rudel, T. (2015). Modulation of p53 during bacterial infections. Nat. Rev. Microbiol. *13*, 741–748. https://doi.org/10.1038/nrmicro3537.

20. Dougan, G., and Baker, S. (2014). Salmonella enterica serovar Typhi and the pathogenesis of typhoid fever. Annu. Rev. Microbiol. *68*, 317–336. https://doi.org/10.1146/annurev-micro-091313-103739.

21. Spanò, S., Ugalde, J.E., and Galán, J.E. (2008). Delivery of a Salmonella Typhi exotoxin from a host intracellular compartment. Cell Host Microbe *3*, 30–38. https://doi.org/10.1016/j.chom.2007.11.001.

22. Song, J., Gao, X., and Galán, J.E. (2013). Structure and function of the Salmonella Typhi chimaeric A(2)B(5) typhoid toxin. Nature *499*, 350–354. https://doi.org/10.1038/nature12377.

23. Ibler, A.E.M., ElGhazaly, M., Naylor, K.L., Bulgakova, N.A., F El-Khamisy, S., and Humphreys, D. (2019). Typhoid toxin exhausts the RPA response to DNA replication stress driving senescence and Salmonella infection. Nat. Commun. *10*, 4040. https://doi.org/10.1038/s41467-019-12064-1.

24. Martin, O.C.B., Bergonzini, A., Lopez Chiloeches, M., Paparouna, E., Butter, D., Theodorou, S.D.P., Haykal, M.M., Boutet-Robinet, E., Tebaldi, T., Wakeham, A., et al. (2021). Influence of the microenvironment on modulation of the host response by typhoid toxin. Cell Rep. *35*, 108931. https://doi.org/10.1016/j.celrep.2021.108931.

25. den Bakker, H.C., Moreno Switt, A.I., Govoni, G., Cummings, C.A., Ranieri, M.L., Degoricija, L., Hoelzer, K., Rodriguez-Rivera, L.D., Brown, S., Bolchacova, E., et al. (2011). Genome sequencing reveals diversification of virulence factor content and possible host adaptation in distinct subpopulations of Salmonella enterica. BMC Genom. *12*, 425. https://doi.org/10.1186/1471-2164-12-425.

26. Miller, R.A., Betteken, M.I., Guo, X., Altier, C., Duhamel, G.E., and Wiedmann, M. (2018). The Typhoid Toxin Produced by the Nontyphoidal Salmonella enterica Serotype Javiana Is Required for Induction of a DNA Damage Response In Vitro and Systemic Spread In Vivo. mBio *9*, e00467-18. https://doi.org/10.1128/mBio.00467-18.

27. Del Bel Belluz, L., Guidi, R., Pateras, I.S., Levi, L., Mihaljevic, B., Rouf, S.F., Wrande, M., Candela, M., Turroni, S., Nastasi, C., et al. (2016). The Typhoid Toxin Promotes Host Survival and the Establishment of a Persistent Asymptomatic Infection. PLoS Pathog. *12*, e1005528. https://doi.org/10.1371/journal.ppat.1005528.

28. Gibani, M.M., Jones, E., Barton, A., Jin, C., Meek, J., Camara, S., Galal, U., Heinz, E., Rosenberg-Hasson, Y., Obermoser, G., et al. (2019). Investigation of the role of typhoid toxin in acute typhoid fever in a human challenge model. Nat. Med. *25*, 1082–1088. https://doi.org/10.1038/s41591-019-0505-4.

29. Mathiasen, S.L., Gall-Mas, L., Pateras, I.S., Theodorou, S.D.P., Namini, M.R.J., Hansen, M.B., Martin, O.C.B., Vadivel, C.K., Ntostoglou, K., Butter, D., et al. (2021). Bacterial genotoxins induce T cell senescence. Cell Rep. *35*, 109220. https://doi.org/10.1016/j.celrep.2021.109220.

30. McGourty, K., Thurston, T.L., Matthews, S.A., Pinaud, L., Mota, L.J., and Holden, D.W. (2012). Salmonella inhibits retrograde trafficking of mannose-6-phosphate receptors and lysosome function. Science *338*, 963–967. https://doi.org/10.1126/science.1227037.

31. Knodler, L.A., Crowley, S.M., Sham, H.P., Yang, H., Wrande, M., Ma, C., Ernst, R.K., Steele-Mortimer, O., Celli, J., and Vallance, B.A. (2014). Noncanonical inflammasome activation of caspase-4/caspase-11 mediates epithelial defenses against enteric bacterial pathogens. Cell Host Microbe *16*, 249–256. https://doi.org/10.1016/j.chom.2014.07.002.

32. Xu, H., Yang, J., Gao, W., Li, L., Li, P., Zhang, L., Gong, Y.N., Peng, X., Xi, J.J., Chen, S., et al. (2014). Innate immune sensing of bacterial modifications of Rho GTPases by the Pyrin inflammasome. Nature *513*, 237–241. https://doi.org/10.1038/nature13449.

33. Pons, B.J., Pettes-Duler, A., Naylies, C., Taieb, F., Bouchenot, C., Hashim, S., Rouimi, P., Deslande, M., Lippi, Y., Mirey, G., and Vignard, J. (2021). Chronic exposure to Cytolethal Distending Toxin (CDT) promotes a cGAS-dependent type I interferon response. Cell. Mol. Life Sci. *78*, 6319–6335. https://doi.org/10.1007/s00018-021-03902-x.

34. Basisty, N., Kale, A., Jeon, O.H., Kuehnemann, C., Payne, T., Rao, C., Holtz, A., Shah, S., Sharma, V., Ferrucci, L., et al. (2020). A proteomic atlas of senescence-associated secretomes for aging biomarker development. PLoS Biol. *18*, e3000599. https://doi.org/10.1371/journal.pbio.3000599.

35. Eichelbaum, K., Winter, M., Berriel Diaz, M., Herzig, S., and Krijgsveld, J. (2012). Selective enrichment of newly synthesized proteins for quantitative secretome analysis. Nat. Biotechnol. *30*, 984–990. https://doi.org/10.1038/nbt.2356.

36. Uhlén, M., Karlsson, M.J., Hober, A., Svensson, A.S., Scheffel, J., Kotol, D., Zhong, W., Tebani, A., Strandberg, L., Edfors, F., et al. (2019). The human secretome. Sci. Signal. *12*, eaaz0274. https://doi.org/10.1126/scisignal.aaz0274.

37. Tominaga, K., and Suzuki, H.I. (2019). TGF-beta Signaling in Cellular Senescence and Aging-Related Pathology. Int. J. Mol. Sci. *20*, 5002. https://doi.org/10.3390/ijms20205002.

38. Guo, Y., Ayers, J.L., Carter, K.T., Wang, T., Maden, S.K., Edmond, D., Newcomb P, P., Li, C., Ulrich, C., Yu, M., and Grady, W.M. (2019). Senescence-associated tissue microenvironment promotes colon cancer formation through the secretory factor GDF15. Aging Cell *18*, e13013. https://doi.org/10.1111/acel.13013.

39. Ha, G., De Torres, F., Arouche, N., Benzoubir, N., Ferratge, S., Hatem, E., Anginot, A., and Uzan, G. (2019). GDF15 secreted by senescent endothelial cells improves vascular progenitor cell functions. PLoS One *14*, e0216602. https://doi.org/10.1371/journal.pone.0216602.

40. Pence, B.D., Yarbro, J.R., and Emmons, R.S. (2021). Growth differentiation factor-15 is associated with age-related monocyte dysfunction. Aging Med. *4*, 47–52. https://doi.org/10.1002/agm2.12128.

41. Zhang, Y.G., Singhal, M., Lin, Z., Manzella, C., Kumar, A., Alrefai, W.A., Dudeja, P.K., Saksena, S., Sun, J., and Gill, R.K. (2018). Infection with enteric pathogens Salmonella typhimurium and Citrobacter rodentium modulate TGF-beta/Smad signaling pathways in the intestine. Gut Microb. *9*, 326–337. https://doi.org/10.1080/19490976.2018.1429878.

42. Williams, K., Gokulan, K., Shelman, D., Akiyama, T., Khan, A., and Khare, S. (2015). Cytotoxic mechanism of cytolethal distending toxin in nontyphoidal Salmonella serovar (Salmonella Javiana) during macrophage infection. DNA Cell Biol. *34*, 113–124. https://doi.org/10.1089/dna.2014.2602.

43. Kwon, M., Leibowitz, M.L., and Lee, J.H. (2020). Small but mighty: the causes and consequences of micronucleus rupture. Exp. Mol. Med. *52*, 1777–1786. https://doi.org/10.1038/s12276-020-00529-z.

44. Borcherding, N., Kusner, D., Kolb, R., Xie, Q., Li, W., Yuan, F., Velez, G., Askeland, R., Weigel, R.J., and Zhang, W. (2015). Paracrine WNT5A Signaling Inhibits Expansion of Tumor-Initiating Cells. Cancer Res. *75*, 1972–1982. https://doi.org/10.1158/0008-5472.CAN-14-2761.

45. Humphreys, D., Davidson, A., Hume, P.J., and Koronakis, V. (2012). Salmonella virulence effector SopE and Host GEF ARNO cooperate to recruit and activate WAVE to trigger bacterial invasion. Cell Host Microbe *11*, 129–139. https://doi.org/10.1016/j.chom.2012.01.006.

46. Jochems, F., Thijssen, B., De Conti, G., Jansen, R., Pogacar, Z., Groot, K., Wang, L., Schepers, A., Wang, C., Jin, H., et al. (2021). The Cancer SENESCopedia: A delineation of cancer cell senescence. Cell Rep. *36*, 109441. https://doi.org/10.1016/j.celrep.2021.109441.

47. Deng, L., Song, J., Gao, X., Wang, J., Yu, H., Chen, X., Varki, N., Naito-Matsui, Y., Galán, J.E., and Varki, A. (2014). Host Adaptation of a Bacterial Toxin from the Human Pathogen Salmonella Typhi. Cell *159*, 1290–1299. https://doi.org/10.1016/j.cell.2014.10.057.

48. Olson, M., and Julian, L. (2015). Apoptotic membrane dynamics in health and disease. Cell Health Cytoskeleton *7*, 133–142. https://doi.org/10.2147/Chc.S57893.

49. Zhang, Y., Alexander, P.B., and Wang, X.F. (2017). TGF-beta Family Signaling in the Control of Cell Proliferation and Survival. Cold Spring Harbor Perspect. Biol. *9*, a022145. https://doi.org/10.1101/cshperspect.a022145.

50. Webster, M.R., Xu, M., Kinzler, K.A., Kaur, A., Appleton, J., O'Connell, M.P., Marchbank, K., Valiga, A., Dang, V.M., Perego, M., et al. (2015). Wnt5A promotes an adaptive, senescent-like stress response, while continuing to drive invasion in melanoma cells. Pigment Cell Melanoma Res. *28*, 184–195. https://doi.org/10.1111/pcmr.12330.

51. Zhao, Y., Wu, Z., Chanal, M., Guillaumond, F., Goehrig, D., Bachy, S., Principe, M., Ziverec, A., Flaman, J.M., Collin, G., et al. (2020). Oncogene-Induced Senescence Limits the Progression of Pancreatic Neoplasia through Production of Activin A. Cancer Res. *80*, 3359–3371. https://doi.org/10.1158/0008-5472.CAN-19-3763.

52. Miyoshi, H., Ajima, R., Luo, C.T., Yamaguchi, T.P., and Stappenbeck, T.S. (2012). Wnt5a potentiates TGF-beta signaling to promote colonic crypt regeneration after tissue injury. Science *338*, 108–113. https://doi.org/10.1126/science.1223821.

53. Almeida, M., Han, L., Bellido, T., Manolagas, S.C., and Kousteni, S. (2005). Wnt proteins prevent apoptosis of both uncommitted osteoblast progenitors and differentiated osteoblasts by beta-catenin-dependent and -independent signaling cascades involving Src/ERK and phosphatidylinositol 3-kinase/AKT. J. Biol. Chem. *280*, 41342–41351. https://doi.org/10.1074/jbc.M502168200.

54. Griesmann, H., Ripka, S., Pralle, M., Ellenrieder, V., Baumgart, S., Buchholz, M., Pilarsky, C., Aust, D., Gress, T.M., and Michl, P. (2013). WNT5A-NFAT signaling mediates resistance to apoptosis in pancreatic cancer. Neoplasia *15*, 11–22. https://doi.org/10.1593/neo.121312.

55. Mill, C., Monk, B.A., Williams, H., Simmonds, S.J., Jeremy, J.Y., Johnson, J.L., and George, S.J. (2014). Wnt5a-induced Wnt1-inducible secreted protein-1 suppresses vascular smooth muscle cell apoptosis induced by oxidative stress. Arterioscler. Thromb. Vasc. Biol. *34*, 2449–2456. https://doi.org/10.1161/ATVBAHA.114.303922.

56. Bo, H., Gao, L., Chen, Y., Zhang, J., and Zhu, M. (2016). Upregulation of the expression of Wnt5a promotes the proliferation of pancreatic cancer cells in vitro and in a nude mouse model. Mol. Med. Rep. *13*, 1163–1171. https://doi.org/10.3892/mmr.2015.4642.

57. Maiti, G., Naskar, D., and Sen, M. (2012). The Wingless homolog Wnt5a stimulates phagocytosis but not bacterial killing. Proc. Natl. Acad. Sci. USA *109*, 16600–16605. https://doi.org/10.1073/pnas.1207789109.

58. Jati, S., Kundu, S., Chakraborty, A., Mahata, S.K., Nizet, V., and Sen, M. (2018). Wnt5A Signaling Promotes Defense Against Bacterial Pathogens by Activating a Host Autophagy Circuit. Front. Immunol. *9*, 679. https://doi.org/10.3389/fimmu.2018.00679.

59. Bradley, S.F., and Kauffman, C.A. (1990). Aging and the response to Salmonella infection. Exp. Gerontol. *25*, 75–80.

60. Ames, W.R., and Robins, M. (1943). Age and Sex as Factors in the Development of the Typhoid Carrier State, and a Method for Estimating Carrier Prevalence. Am. J. Public Health Nation's Health *33*, 221–230. https://doi.org/10.2105/ajph.33.3.221.

61. Lim, J.S., Choy, H.E., Park, S.C., Han, J.M., Jang, I.S., and Cho, K.A. (2010). Caveolae-mediated entry of Salmonella typhimurium into senescent nonphagocytotic host cells. Aging Cell *9*, 243–251. https://doi.org/10.1111/j.1474-9726.2010.00554.x.

62. Mirzayans, R., Andrais, B., Hansen, G., and Murray, D. (2012). Role of p16(INK4A) in Replicative Senescence and DNA Damage-Induced Premature Senescence in p53-Deficient Human Cells. Biochem. Res. Int. *2012*, 951574. https://doi.org/10.1155/2012/951574.

STAR★METHODS

KEY RESOURCES TABLE

REAGENT or RESOURCE	SOURCE	IDENTIFIER
Antibodies		
γH2AX (ser-139) (1:1000)	Merck	Cat# 05–636; RRID:AB_2924829
RPApT21 (1:1000)	Abcam	Cat# ab61065; RRID:AB_946322
53BP1 (1:1000)	Novus Biotechnology	Cat# NB100-304; RRID:AB_10003037
P21 Waf1/Cip1 (12D1) (1:500)	Cell Signaling Technology	Cat# 2947; RRID:AB_823586
Phospho-Rb (Ser807/811) (1:500)	Cell Signaling Technology	Cat# 8516; RRID:AB_11178658
SMAD2/3 (D7G7) (1:500)	Cell Signaling Technology	Cat# 8685; RRID:AB_10889933
ATM (Ab-2) (:500)	Millipore	Cat# OP90-200UG; RRID:AB_213436
ATR (C-1) (1:500)	Santa Cruz	Cat# sc-515173; RRID:AB_2893291
Tubulin (1:500)	Abcam	Cat# ab7291; RRID:AB_2241126
phospho-smad 2 (Ser465/467) (1:500)	Cell Signaling Technology	Cat# 3108; RRID:AB_490941
phospho-smad1/5 (Ser463/465) (1:500)	Cell Signaling Technology	Cat# 9516; RRID:AB_491015
INHBA (1:500)	Novus Biotechnology	Cat# NBP1-30928; RRID:AB_2125870
INHBA (1:500)	Thermofisher	Cat# PA5-21939; RRID:AB_11153440
INHBA (1:500)	R&D Systems	Cat# MAB8649; RRID:AB_2916058
Wnt5a (1:500)	Abcam	Cat# ab179824; RRID:AB_2924384
Wnt5a (1:500)	Thermo Fisher Scientific	Cat# MA5-15502; RRID:AB_10985211
Wnt5a/b (1:500)	Cell Signaling Technology	Cat# 9516; RRID:AB_491015
GDF15 (1:500)	Atlas Antibodies	Cat# HPA011191; RRID:AB_1078962
anti-rabbit 568 IgG, Alexa Fluor (1:500)	Thermo Fisher Scientific	Cat# A-11036; RRID:AB_10563566
anti-mouse 488 IgG, Alexa Fluor (1:500)	Molecular Probes	Cat# A-21202; RRID:AB_141607
anti-rabbit 488 IgG, Alexa Fluor (1:500)	Thermo Fisher Scientific	Cat# A-11008; RRID:AB_143165
anti-mouse 594 IgG, Alexa Fluor (1:500)	Molecular Probes	Cat# A-21203; RRID:AB_141633
anti-ms 647 IgG, Alexa Fluor (1:500)	Molecular Probes	Cat# A-21240; RRID:AB_141658
FLAG M2 (1:1000)	Sigma-Aldrich	Cat# F3165; RRID:AB_259529
Myc (1:1000)	GenScript	Cat# A00172; RRID:AB_914457
His (1:1000)	Cell Signaling Technology	Cat# 2365; RRID:AB_2115720
Bacterial and virus strains		
S. Javiana WT	Ref. 26	S5-0395
S. Javiana ΔcdtB	Ref. 26	M8-0540
Chemicals, peptides, and recombinant proteins		
Gentamicin sulfate	Santa Cruz	sc203334
Penicillin/Streptomycin	Gibco	11548876
Kanamycin sulfate	BioBasic	KB0286
Ampicillin	Melford Lab	A0104
Aphidicolin	Sigma-Aldrich	A0781
Etoposide	Cayman Chemicals	12092
TGF-β RI Kinase Inhibitor III	Sigma-Aldrich	616453
KU55933 (ATM inhibitor)	AOBIOUS, INC	AOB2108
ATR inhibitor	Laboratory of Sherif ElKhamisy	AZD6738
TGFB3	Cell Signaling Technology	8425LC
GDF15	R&D Systems	957-GD-025
Wnt5a	R&D Systems	645-WN
INHBA	R&D Systems	338-AC-010

(*Continued on next page*)

Continued

REAGENT or RESOURCE	SOURCE	IDENTIFIER
Epidermal Growth Factor (EGF)	Merck	GF144
Leupeptin	Sigma-Aldrich	62070
Pepstatin	Sigma-Aldrich	77170
Chymostatin	Sigma-Aldrich	C7268
Tris(2-carboxyethyl)phosphine hydrochloride solution (TCEP)	Merck	646547
Sodium dodecyl sulfate (SDS) solution for mass spectrometry	Sigma-Aldrich	5030
Triethylamonium bicarbonate (TEAB)	Thermofisher	Sigma-Aldrich
Iodoacetamide	Sigma-Aldrich	I6125
Pierce MS grade trypsin	Fisher Scientific	3464189
Formic acid	Fisher Scientific	A117-50
Acetonitrile	Sigma-Aldrich	900667
Methanol, UHPLC	Sigma-Aldrich	900688
Water, Optima™ LC/MS Grade, Fisher Chemical™	Thermo Scientific™	W6-1
Halt™ Protease and Phosphatase Inhibitor Cocktail (100X)	Thermo Scientific™	78440
Phorbol 12-myristate 13-acetate (PMA)	Sigma-Aldrich	P8139
Dulbecco's Modified Eagle's Medium (DMEM)	Sigma-Aldrich	Sigma-Aldrich
RPMI-1640	Sigma-Aldrich	R8758
OptiMEM reduced serum	Gibco	31985–047
GlutaMAX supplement	Gibco	35050–61
HEPES (1 M)	Gibco	15630080
Fetal bovine serum (FBS)	Sigma-Aldrich	F7524
L-glutamine	Thermo Scientific™	25030032
MEM Non-Essential Amino Acids Solution (NEAA)	Gibco	11140050
Bovine Serum Albumin Fraction V	Merck	1073508600
Triton X-100	VWR	8817.295
Paraformaldehyde	Sigma-Aldrich	P6148
Phosphate Buffered Saline (PBS, 10X)	Scientific Laboratory Supplies	P5493-4L
Dulbecco′s Phosphate Buffered Saline (Sterile)	Merck	D8537
Critical commercial assays		
CellEvent Senescence Green	Invitrogen	C10851
Click-iTTM EdU Cell Proliferation Kit for Imaging, Alexa FluorTM 647 dye	Thermofisher	C10340
Senescence β-Galactosidase Staining Kit	Cell Signaling Technology	9860S
Apotracker™ Green	BioLegend	427403
LIVE/DEAD™ Viability/Cytotoxicity Kit	Invitrogen	L3224
QuikChange II Site-Directed Mutagenesis Kit	Agilent	200523
Deposited Data		
TxWT induced changes in the host cell secretome	This study, ProteomeXchange Consortium	ProteomeXchange: PXD037373
TxWT induced transcriptional changes in host cells	This study, ArrayExpress	ArrayExpress: E-MTAB-12333
FIJI image processing macros	This study, GitHub	https://doi.org/10.5281/zenodo.8325045
Experimental models: Cell lines		
HT1080	ATCC	CCL-121

(*Continued on next page*)

Continued

REAGENT or RESOURCE	SOURCE	IDENTIFIER
IMR90	Coriell Institute	I90
NIH/3T3	Laboratory of Kai Erdmann	N/A
HIEC-6	ATCC	CRL-3266
THP1	ATCC	TIB-202™
HCT116	ATCC	CCL-247
Oligonucleotides		
ON-TARGETplus SMARTpool Non-targeting Control	Horizon Discovery	D-001810-01-20
ON-TARGETplus SMARTpool ATM	Horizon Discovery	L-003201-00-0005
ON-TARGETplus SMARTpool ATR	Horizon Discovery	L-003202-00-0005
ON-TARGETplus SMARTpool Wnt5a	Horizon Discovery	L-003939-00-0005
ON-TARGETplus SMARTpool Smad2	Horizon Discovery	L-003561-00-0005
ON-TARGETplus SMARTpool INHBA	Horizon Discovery	L-011701-00-0005
ON-TARGETplus SMARTpool GDF15	Horizon Discovery	L-019875-00-0005
ON-TARGETplus Wnt5a Set of 4 siRNA	Horizon Discovery	#1: J-003939-09-0002 #2: J-003939-10-0002 #3: J-003939-11-0002 #4: J-003939-12-0002
ON-TARGETplus INHBA Set of 4 siRNA	Horizon Discovery	#1: J-011701-06-0002 #2: J-011701-07-0002 #3: J-011701-08-0002 #4: J-011701-09-0002
ON-TARGETplus SMAD2 Set of 4 siRNA	Horizon Discovery	#1: J-003561-05-0002 #2: J-003561-06-0002 #3: J-003561-07-0002 #4: J-003561-08-0002
Recombinant DNA		
plasmid 319	pET-Duet1 encoding pltBHis pltAMyc and cdtBFLAG	Ref. 23
plasmid 321	319 with H160Q mutation in cdtB	Ref. 23
plasmid 342	319 with S35A mutation in pltB	This study
Primers for site-directed mutagenesis of PltBS35A	194_PltB_S35A_Forward primer: 5′-GGAGATAATACGAACGCCG CCTACGCGGACGAAG-3′, 195_PltB_S35A_Reverse primer: 3′-CTTCGTCCGCGTAGGCGGC GTTCGTATTATCTCC-5	This study
Software and algorithms		
Graphpad Prism 9.0.0	Graphpad by Dotmatics	https://www.graphpad.com
FIJI 2.0.0-rc-69/1.52p	ImageJ Wiki	https://ImageJ.net/software/fiji/
Microsoft Excel	Microsoft	https://www.microsoft.com/en-gb/
CellProfiler	Broad Institute	https://cellprofiler.org
Perseus version 1.5.6.0	Max-Planck-Institute of Biochemistry	https://maxquant.net/perseus/
MaxQuant version 1.6.10.43	Max-Planck-Institute of Biochemistry	https://maxquant.net/maxquant/
Adobe Illustrator 2021	Adobe	https://www.adobe.com/uk/
Other		
Lipofectamine RNAiMax	Invitrogen	13778–150
S-trap columns	Protifi	C02
VectaShield mounting agent with DAPI	Vector Lab	H1200
Amicon filters (3 kDa cutoff)	Merck	ufc900324
NiNTA agarose	Qiagen	30210
Syringe filter (0.2 μm)	Sarstedt	83.1826.001

RESOURCE AVAILABILITY

Lead contact

Further information and requests for resources and reagents should be directed to and will be fulfilled by the lead contact, Daniel Humphreys (d.humphreys@sheffield.ac.uk).

Materials availability

Plasmids generated in this study (STAR Methods Table) will be shared upon request to the lead contact with a completed Materials Transfer Agreement.

Data and code availability

- Access original data. The mass spectrometry data have been deposited at the ProteomeXchange Consortium via the PRIDE partner repository. The GeneChip Microarray data can be found on ArrayExpress. Accession numbers are listed in the key resources table.
- Access original code. Original code for semi-automated image processing has been deposited on Zenodo via GitHub. DOI is listed in the key resources table.
- Access any additional information required to reanalyse the data reported in this paper is available from the lead contact upon request.

EXPERIMENTAL MODEL AND SUBJECT PARTICIPANT DETAILS

Cell lines and maintenance

Cells were maintained in a humidified incubator (Panasonic, MCO-170AICUV-PE) at 37°C and 5% CO2. Cells were passaged every 2–3 days in their appropriate media. HT1080 (ATCC, CCL-121), NIH/3T3, and IMR90 (Coriell, I90) cells were cultured in Dulbecco's Modified Eagle's Medium (DMEM; Sigma Aldrich, D6546); THP1 (ATCC, TIB-202) and HCT116 (ATCC, CCL-247) cells in RPMI1640 (Sigma-Aldrich, R8758); and HIEC-6 in Opti-MEM Reduced Serum Medium (Gibco, 31985-047). To make complete growth media for HT1080 and NIH3T3, basal media were supplemented with: 2mM L-glutamine (Thermo Scientific, 25030032), and 10% fetal bovine serum (FBS, Sigma-Aldrich F7524). For THP1 and HCT116, basal media was supplemented with 10% FBS. For IMR90 cells: 15% FBS, 1% non-essential amino acids (Gibco, 11140050), and 1% GlutaMAX (Gibco, 35050-61). For HIEC-6: 20 mM HEPES (Gibco, 15630080), 10 mM GlutaMAX, 10 ng/mL epidermal growth factor (EGF; Merck GF144) and 4% FBS. All base media were supplemented with 10 U/ml Penicillin/Streptomycin (Gibco, 11548876) and 50 μg/mL Kanamycin sulfate (BioBasic, KB0286),or 100 μg/mL Ampicillin (Melford, A0104) only if used in infection assays. To differentiate THP1 cells to macrophages, 100 ng/mL Phorbol 12-myristate 13-acetate (PMA; Sigma-Aldrich P8139) was added for 72 h.

Salmonella strains

Wild-type *Salmonella enterica* serovar Javiana (isolate S5-0395) and the isogenic null mutant Δ*cdtB* (isolate M8-0540) were kind gifts from Prof. Martin Weidmann (New York). *S.*Javiana were cultured on Luria broth (LB) agar plates overnight at 37°C then stored at 4°C and sub-cultured every 7–10 days.

METHOD DETAILS

Toxin purification and intoxication

The typhoid toxin was purified from BL21 DE3 pETDuet-1 encoding $pltB^{His}$ $pltA^{Myc}$ and $cdtB^{FLAG}$ using NiNTA agarose (Qiagen) affinity chromatography according to manufacturer instructions as previously described (23). The S35A mutation in *pltB* was generated by amplifying plasmid 319 with primers 194/195 using the QuikChange II Site-Directed Mutagenesis Kit according to manufacturer instructions (Agilent). Unless stated otherwise, cells were intoxicated with 20 ng/ml toxin (~175 pM) for 2h, washed three times with sterile PBS to remove any extracellular toxin and chased with fresh complete growth media for the duration of the experiment.

Cell culture treatments

Cells were treated with 20 μM APH or 10 μM ETP for 24 h prior to washing 3X with PBS and incubating with fresh complete growth medium. TGF-β RI Kinase Inhibitor III, KU55933 (ATM inhibitor) and AZD6738 (ATR inhibitor) were added at 1 μM after washing the toxin off or in conditioned media. Purified ligands were added to cells following optimisation in the respective cell types below as follows: 10 ng/mL TGFB3 for pSMAD2 signaling, and 0.5 μg/ml INHBA and 0.5 μg/ml Wnt5a for paracrine senescence in HT1080 fibroblasts; 0.2 μg/ml GDF15 and 0.05 μg/ml Wnt5a for *Salmonella* invasion experiments in THP1 macrophages. When assaying cellular senescence, growth media supplemented with ligands were incubated with HT1080 fibroblasts for 120h (unless stated otherwise). When assaying *Salmonella* invasion, THP1 macrophages in serum-free growth media were supplemented with ligands followed by immediate addition of *Salmonella* for 30 min to initiate infection as described in the *Salmonella* infection assay. For

neutralisation assays, neutralising antibodies against proteins of interest were incubated in conditioned media at 1:1000 dilution on a rotator for 1h at 37C prior to treating the cells for indicated time-points.

siRNA transfection

Per well of a 24-well plate format (i.e., for fluorescence microscopy), Lipofectamine RNAiMax (0.25 μL or 0.5 μL) and siRNA (0.5 μL of 20 μM stock) were prepared in two different tubes of 25 μL OptiMEM media, then mixed together for 5 min at room temperature. The 50 μL mix of siRNA and lipofectamine were added to 450 μL complete growth DMEM and incubated on cells for 48h. Per well of a 6-well plate (i.e., for immunoblotting), 3 μL of Lipofectamine RNAiMax and 1.5 μL siRNA used in 125 μL OptiMEM media each. They were then mixed and added to 1.25 mL of cell culture media. The final concentration of siRNA in culture was 20 nM. Unless otherwise stated, cells were intoxicated for 2h followed immediately by 48h transfection with indicated siRNAs. When secretomes were harvested from Wnt5a-depleted cells for downstream assays, cells were transfected with siRNAs targeting Wnt5a expression 48h prior to an intoxication assay (i.e., 2h TxWT treatment, 3x washes with PBS, 48h chase with fresh media). This ensured the conditioned media did not contain siRNAs that could complicate interpretation in naive cells treated Wnt5a-depleted secretomes.

Salmonella infection

*S.*Javiana (S5-0395) and Δ*cdtB* (M8-0540) encoding pM975, which express GFP when bacteria are intracellular(57), were cultured in LB 50 μg/ml ampicillin at 37°C in a shaking incubator to 2.0 OD600. The multiplicity of infection (MOI) was optimised for THP1 cells (MOI 20), HT1080 cells (MOI 50), and NIH3T3cells (MOI 160). To assay *Salmonella*-induced SMAD2 signaling, infection was initiated in the absence of antibiotics by addition of *Salmonella* to cell cultures in complete growth medium and centrifugation for 1 min at 1000 × g followed by 30 min incubation at 37°C 5% CO_2. Infected cells were washed three times with PBS and incubated in growth media containing 50 μg/mL gentamicin (Chem Cruz, sc203334) for 1.5h then reduced to 10 μg/mL gentamicin for the rest of the experiment. When assaying *Salmonella* invasion, the method was modified by serum-starving cells 24h prior to infection that deprives cells of membrane ruffling stimulants in FBS. To assess the effect of txSASP on invasion, media was replaced with conditioned media or fresh serum-free media containing purified ligands before immediate addition of *Salmonella* to initiate infection over 30 min. After 1.5h incubation with 50 μg/mL gentamicin, cells were washed three times with PBS and lysed with 1% Triton X-100. Serial dilutions of cell lysates were used to inoculate (5 μL) LB agar plates containing 50 μg/ml ampicillin and the *Salmonella* cultured overnight at 37°C. *Salmonella* colony counts were used to quantify colony forming units (CFUs).

Immunoblotting

Whole cell lysates were generated by re-suspending cultured cells in SDS-UREA (50 mM Tris pH 6.8, 8M Urea, 2% SDS, 0.3% Bromo blue). For immunoblotting pSMAD2, cells were lysed in RIPA buffer (50 mM Tris pH7.4, 150 mM NaCl, 1.0% NP-40, 0.5% sodium deoxycholate, 0.1% SDS) supplemented with Thermo Scientific Halt Protease and Phosphatase Inhibitor Cocktail (#78440) and diluted 1:1 with 2X Laemmli buffer (125 mM Tris-HCl pH 6.8, 20% glycerol, 10% βmercaptoethanol, 4% SDS, 0.5% bromophenol blue). Proteins were separated by 9% Bis-Tris SDS-PAGE gels in MOPS buffer (50 mM MOPS, 50 mM Tris, 0.1% SDS, 20 mM EDTA) and transferred to PVDF transfer stacks (#1704274, Bio-Rad) using Trans-Blot Turbo Transfer System (Bio-Rad). PVDF membranes were blocked with TBS pH7.4 5% non-fat dried milk with antibody incubations and washes performed in TBS pH7.4 0.1% Tween 20. IRDye-labelled secondary antibodies were used according to manufacturer's instructions and immunoblots imaged using Odyssey Sa (LiCor).

Immunofluorescence

Media was washed off with PBS, then fixed with 4% paraformaldehyde (PFA) in PBS for 10–15 min at room temperature. Cells were washed two more times with PBS (Biotech, PD8117) then blocked and permeabilised using a 3% BSA (Sigma-Aldrich, 1073508600), 0.2% Triton X-100 (VWR, 28817.295) in PBS, at room temperature for 1h. Primary and secondary antibodies were added in blocking buffer consecutive for 1h and 30min, respectively then washed with PBS then water and left to dry. Coverslips were then mounted and counterstained on 6 μL of VectaShield mounting agent with DAPI (Vector Lab, H1200), and sealed before being imaged on Nikon's Inverted Ti eclipse equipped with an Andor Zyla sCMOS camera (2560 x 2160; 6.5μm pixels). The objectives used were Plan Apo 10× (NA 0.45); Plan Apo 20x (NA 0.75); Plan Fluor 40x oil (NA 1.3); Apo 60x oil (NA 1.4); Plan Apo 100x Ph oil (Na 1.45); Plan Apo VC 100x oil (NA 1.4). Quad emission filters for used with SpectraX LED excitation (395nm, 470nm, 561nm, 640nm). The imaging software used was NIS elements software. Two antibodies were used for immunofluorescence of INHBA, i.e., Figures 2B and 4G, S5G (Cat# NBP1-30928), Figure 4H (Cat# MAB8649).

Senescence assays

Senescence was assayed by histological staining using Senescence β-Galactosidase Staining Kit (Cell Signaling Technology #9860S), or fluorescence using CellEvent Senescence Green Probe (Invitrogen, C10851) as per the manufacturer's instructions. To assay for cell-cycle arrest, Click-iT EdU Cell Proliferation Kit for Imaging, Alexa FluorTM 647 dye (Thermofisher, C10340) was used per the manufacturer's instruction. For example, HT1080 duplication time is 18h, therefore EdU was added to the culture 24h before fixation. Where EdU were to be co-stained with CellEvent Green and other immunofluorescence staining, the order of assays was CellEvent Senescence Green, EdU staining Kit, and then immunofluorescence. Histological SA-β-gal was imaged using

the inverted microscope Nikon Eclipse Ts2 equipped with sCMOS Ds-Fi-3 camera with built-in Diascopic, high-intensity LED illumination system at 10x and 20x objective lenses.

Survival assays

LIVE/DEAD Viability/Cytotoxicity Kit, for mammalian cells (Invitrogen, L3224) was used as per the manufacturer's instructions. Briefly, 2X mixture of calcein AM (1:2000; live dye) and ethidium homodimer-1 (1:500; dead dye). Cells were washed two times in PBS then the live/dead solution was added 1:1 on cells for 30 min. Cells were treated with 70% methanol for 30 min as a positive control for dead cells. Cells were imaged on the inverted microscope Nikon Eclipse Ts2 equipped with sCMOS Ds-Fi-3 camera with built-in Diascopic, high-intensity LED illumination system at 10x and 20x objective lenses. To identify apoptotic cells, Apotracker Green was used as per the manufacturer's instructions. Briefly, apotracker was added to cell culture media at 0.2 μM for 45 min, then fixed using 4% PFA for 15 min. Cells were imaged on Nikon's Inverted Ti eclipse equipped with an Andor Zyla sCMOS camera (2560 x 2160; 6.5μm pixels). The objectives used were Plan Fluor 40× oil (NA 1.3); Plan Apo 100x Ph oil (Na 1.45). Quad emission filters for used with SpectraX LED excitation (395nm, 470nm). The imaging software used was NIS elements software.

Secretome harvest and paracrine senescence

Conditioned media was centrifuged at 6000 × g for 5 min to pellet the cells before filtering through 0.2μm filters to prevent cell contamination and release of non-SASP intracellular factors due to the filtration pressure. For proteomic experiments, conditioned media was harvested in the absence of serum, which can mask less abundant proteins in the secretome during LC-MS/MS analysis (e.g., due to the high abundance of albumin in serum). Conditioned media was stored at-80°C. Before incubation with cells for paracrine senescence assays, conditioned media was diluted 1:1 with complete growth media, or if serum-free conditioned media was harvested then media was supplemented with 10% FBS.

GeneChip microarray

Cells were seeded in T75 tissue culture flasks for a 30% confluency before intoxication with txWT and txHQ at 5 ng/ml as described. After 48 h, cells were trypsinised and RNA isolation was carried out. Samples were analyzed at the Sheffield Institute of Translational Neurosciencel (SITraN (kindly supported by Paul Heath) on ClariomS assay, human (ThermoFisher Scientific, 902927). Analysis was performed with Transcriptome Analysis Console 4.0 software (Applied Biosystems, Thermo Fisher Scientific). The dataset can be accessed via ArrayExpress: E-MTAB-12333.

Mass spectrometry-based proteomics

A protease mixture of leupeptin, pepstatin, and chymostatin (Sigma Aldrich, 62070, 77170, C7268, respectively) each at a final concentration of 10 μg/mL) was added to harvested serum-free conditioned media immediately. Samples were concentrated using amicon filters with 3 kDa cutoff down to 250 μL at 4000×g using swing bucket centrifuge at 4°C. 50 μL of the concentrated media was used for S-trap digestion. Equal volume of 2x S-trap lysis buffer containing 10% SDS (Sigma-Aldrich, 05030), 100mM TEAB, pH 7.55 (Thermofisher, 90114) was added to the samples. Next, the samples were reduced by adding TCEP (Merck, 646547) at a final concentration of 10 mM. The samples were then heated at 70°C for 15 min at 750 rpm in a shaking incubator then cooled down for 5 min at room temperature. Next, the samples were alkylated by adding 20 mM iodoacetamide (Merck, I6125) in the dark for 30 min at room temperature. The samples were then acidified by adding aqueous phosphoric acid to a final concentration of 1.2%. S-trap binding buffer (90% aqueous methanol, 0.1M TEAB, pH 7.1) was added to the solution in a ratio of 1:7. Samples were then loaded into the S-trap columns (Protifi, C02), 150 μL at a time and centrifuged at 4000 x g for 10 s to pass through the S-trap. The S-trap was then washed 3X with 150 μL binding buffer before transferring it to a clean 2 mL Eppendorf tube. MS grade trypsin (Fisher Scientific, 13464189) resuspended in 0.1% TFA was then added to a ratio of 1:10 trypsin:protein w/w in 50 mM TEAB buffer. 30 μL of trypsin in TEAB buffer was added to the samples. The S-trap was incubated at 47°C for 1 h without shaking. The peptides were then eluted by adding 40 μL of 50 mM TEAB, 40 μL of 0.2% aqueous formic acid (Fisher Chemical, A117-50) then 40 μL of 50% ACN containing 0.2% aqueous formic acid at 4000×g for 10 s each. Samples were dried in a SpeedVac (Eppendorf) at 45°C for 60–90 min with vacuum setting V-AQ. Peptides were resuspended in 0.5% formic acid and 18 μL of each sample was analyzed by nanoflow LC-MS/MS using an Orbitrap Elite (Thermo Fisher) hybrid mass spectrometer equipped with an easyspray source, coupled to an Ultimate RSLCnano LC System (Dionex). The system was controlled by Xcalibur 3.0.63 (Thermo Fisher) and DCMSLink (Dionex). Peptides were desalted on-line using an Acclaim PepMap 100 C18 nano/capillary BioLC, 100A nanoViper 20 mm × 75 μm I.D. particle size 3 μm (Fisher Scientific) and then separated using a 125-min gradient from 5 to 35% buffer B (0.5% formic acid in 80% acetonitrile) on an EASY-Spray column, 50 cm × 50 μm ID, PepMap C18, 2 μm particles, 100 A pore size (Fisher Scientific). The Orbitrap Elite was operated with a cycle of one MS (in the Orbitrap) acquired at a resolution of 60,000 at m/z 400, with the top 20 most abundant multiply charged (2+ and higher) ions in a given chromatographic window subjected to MS/MS fragmentation in the linear ion trap using CID with a normalised collision energy of 35%. An FTMS target value of 1e6 and an ion trap MSn target value of 1e4 were used with the lock mass (445.120025) enabled. Maximum FTMS scan accumulation time of 200 ms and maximum ion trap MSn scan accumulation time of 50 ms were used. Dynamic exclusion was enabled with a repeat duration of 45 s with an exclusion list of 500 and an exclusion duration of 30 s.

QUANTIFICATION AND STATISTICAL ANALYSIS

Analysis of proteomic data

All raw mass spectrometry data were processed with MaxQuant version 1.6.10.43. Data were searched against a human UniProt sequence database (June 2015) using the following search parameters: digestion set to Trypsin/P with a maximum of 2 missed cleavages, methionine oxidation and N-terminal protein acetylation as variable modifications, cysteine carbamidomethylation as a fixed modification, match between runs enabled with a match time window of 0.7 min and a 20-min alignment time window, label-free quantification enabled with a minimum ratio count of 2, minimum number of neighbors of 3 and an average number of neighbors of 6. A first search precursor tolerance of 20ppm and a main search precursor tolerance of 4.5 ppm was used for FTMS scans and a 0.5 Da tolerance for ITMS scans. A protein FDR of 0.01 and a peptide FDR of 0.01 were used for identification level cut-offs. MaxQuant output was loaded into Perseus version 1.5.6.0 and the matrix was filtered to remove all proteins that were potential contaminants, only identified by site and reverse sequences. LFQ intensities were log2(x) transformed and data was filtered to retain proteins with a minimum of three valid LFQ Intensities in one group. Subsequently, data were visualised using multi-scatter plots and Pearson's correlation analysis. Data were then normalised by subtracting column medians and missing values were imputed from the normal distribution with a width of 0.3 and downshift of 1.8. In order to identify quantitatively enriched proteins between groups, two-sided Student's t-tests were performed with a permutation-based FDR of 0.05 with an S0 = 0.1. Data was then exported into an excel file and input into GraphPad Prism to create the figures and plots presented.

Quantification

Phenotypes in microscopy images were quantified using either CellProfiler 4.2.1 in semi-automated fashion (Quantification Protocols Q1-Q5) or manually using Fiji 2.1.0/1.53c (Q6). Quantification protocols used are cited in each legend. Quantification using CellProfiler 4.2.1: (**Q1**) DAPI-stained nuclei and EdU-labelled objects were detected using IdentifyPrimaryObject module by nominating diameter ranges and an absolute signal threshold, then RelateObjects module was used to automatically determine EdU-positive nuclei. (**Q2**) Nuclei were detected in the same way as Q1 then integrated intensity of the nuclear proteins of interest were measured using the MeasureObject intensity module. Cells were then classified using (a) average or (b) the upper quartile of the negative control measured intensity as a threshold for positive cells. (**Q3**) Cytoplasmic components were quantified using the MeasureImageIntensity module divided by the number of nuclei counted using IdentifyPrimaryObjects. (**Q4**) Nuclei were detected as described in Q1, then foci were detected using IdentifyPrimaryObjects, and then the RelateObjects were used to attribute the number of foci to each nucleus. To identify foci-positive and negative nuclei, threshold was set at average number of foci in untreated cells. Pan-stained nuclei (e.g., γH2AX) were quantified and excluded from foci analysis by selecting them using the EditObjectsManually module. (**Q5**) IdentifySecondaryObjects module was used to expand an area around the nucleus (around 50px for SA-β-gal or Apotracker and 1px for RPApT21). An intensity threshold was manually set, then the MaskObjects was used to identify positive cells based on the fraction of their overlap with the expanded area. Cells were classified into positive or negative using the ClassifyObjects module. Quantification using Fiji: **(Q6)** FIJI cell counter plugin was used and raw numbers were then recorded and processed in Microsoft Excel. Quantification of immunoblots (**Q7**) were carried out using ImageStudio v5.0 where band intensities of target proteins were normalised to loading controls before determining relative band intensities to negative controls.

Image processing

Fiji 2.1.0/1.53c macro code was created to automate processed images. Briefly, brightness and contrast are normalised across all images of interest, a pre-set ROI is used to crop images to regions of interest, and a pre-set scale bar is added. DAPI nuclei are then outlined, overlaid with the other channels and saved as png files. Many variants of the code have been created to cater for 2-channel, 3-channel and 4-channel images, with either normal composite images or with DAPI outlines. The codes can be found via this link: https://drive.google.com/drive/folders/1SwUO-bgyW0rjY9MetAfKGtdd77FsCahF?usp= sharing. Adobe Illustrator was used to manually hand-draw illustrations, and assemble all results figures.

Statistics

Data was recorded and organised in Microsoft Excel. Graphs were generated and statistics were performed using GraphPad Prism 9.0.0. Statistical significance (*) was defined as *$p < 0.05$, **$p < 0.01$, ***$p < 0.001$, ****$p < 0.0001$, ns denotes non-significance. Statistical details can be found in the figure legends including statistical tests and n number (biological replicates). Error bars indicate standard error of the mean (SEM). Each circle in bar charts represents a biological replicate (defined as *n*) from which statistics were performed on at least 3 biological replicates.